Numerical Investigation of Various Heat Transfer Performance Enhancement Configurations for Energy Harvesting Applications

Samruddhi Aniruddha Deshpande

Thesis submitted to the faculty of the
Virginia Polytechnic Institute and State University
in partial fulfillment of the requirements for the degree of

Master of Science
In
Mechanical Engineering

Srinath V. Ekkad, Chair
Scott Huxtable, Co-Chair
Rui Qiao

June 10, 2016
Blacksburg, VA

Keywords: Computational Fluid Dynamics, Heat Transfer, Gas Turbines, Thermoelectric Generators

Numerical Investigation of Various Heat Transfer Performance Enhancement Configurations for Cooling Applications

Samruddhi Aniruddha Deshpande

ABSTRACT

Conventional understanding of quality of energy suggests that heat is a low grade form of energy. Hence converting this energy into useful form of work was assumed difficult. However, this understanding was challenged by researchers over the last few decades. With advances in solar, thermal and geothermal energy harvesting, they believed that these sources of energy had great potential to operate as dependable avenues for electrical power. In recent times, waste heat from automobiles, oil and gas and manufacturing industries were employed to harness power. Statistics show that US alone has a potential of generating 120,000 GWh/year of electricity from oil , gas and manufacturing industries, while automobiles can contribute upto 15,900 GWh/year.

Thermoelectric generators (TEGs) can be employed to capture some of this otherwise wasted heat and to convert this heat into useful electrical energy. This field of research as compared to gas turbine industry has emerged recently over past 30 decades. Researchers have shown that efficiency of these TEGs modules can be improved by integrating heat transfer augmentation features on the hot side of these modules. Gas turbines employ advanced technologies for internal and external cooling. These technologies have applications over wide range of applications, one of which is thermoelectricity. Hence, making use of gas turbine technologies in thermoelectrics would surely improve the efficiency of existing TEGs.

This study makes an effort to develop innovative technologies for gas turbine as well as thermoelectric applications. The first part of the study analyzes heat transfer augmentation from four different configurations for low aspect ratio channels and the second part deal with characterizing improvement in efficiency of TEGs due to the heat transfer augmentation techniques.

ACKNOWLEDGEMENTS

I would like to thank my advisor, Dr. Srinath Ekkad with whose valuable support and encouragement I was able to accomplish this study. This association of working with him has definitely moulded me into a more focused person. I will always remember all the important lessons of patience, hard work that I learnt from him. His enthusiasm and encouraging words will always remind me to be humble in greatest of the achievements.

Dr. Scott Huxtable has also played a crucial role in shaping my master's thesis. I greatly appreciate the endless hours of discussion sessions he devoted to guide me. I thank him for spending hours on rectifying my very first paper publication, considering that I was a novice at it, he helped me understand the correct way to pen down literature. This will surely prove helpful in years to come. I am grateful to Dr. Rui Qiao for conducting a detailed course on convective heat transfer, which is the back bone of this study and providing his valuable insights.

I would like to extend a heartfelt gratitude to Dr. Jaideep Pandit and David Gomez who provided guidance whenever needed and even answer my trivial questions with utmost patience. I would like to acknowledge Sandeep and Sridharan who helped me understand the best practices in Computational Fluid Dynamics. A special mention to Prashant and Bharath for their encouragement and support, your hard work and dedication will always remain an inspiration for me. Last but not the least , I would like to thank all my lab mates - Kris, Kartikeya, Prethive, Siddhartha and Shubham for making this transition from an outsider to a part of HEFT lab so easy for me.

Most importantly I would like to thank my family for support they provided and trust they bestowed in me. Thanks a lot Aaji, Aai, Baba, Mavshi, Kaka, Saniya, Bhargav and Aarohi. Nonetheless, a special thanks to my friends who didn't abandon me for my constant irritation , bickering about job search and several cooking turns that you took on my behalf – Thank you – Surabhi , Surabhi R , Pooja , Aakruthi , Ramachandra , Savio , Abhishek , Rohit , Ajinkya.

TABLE OF CONTENTS

CHAPTER 1

COMPUTATIONAL STUDY OF SPATIALLY RESOLVED HEAT TRANSFER AND FLUID STRUCTURE IN HIGH ASPECT RATIO CHANNELS WITH FOUR DIFFERENT PIN FIN- DIMPLE ARRAY CONFIGURATIONS

Samruddhi A. Deshpande, Jaideep Pandit, Scott Huxtable, Srinath V. Ekkad
Department of Mechanical Engineering
Virginia Polytechnic Institute and State University
Blacksburg, Virginia, USA

To be submitted to the International Journal of Thermal Sciences

ABSTRACT

Short pin fins are typical of applications found in internally cooled gas turbine engine airfoils and electronics industry. Along with high heat transfer potential these pin fins are associated with increased pressure drop. This increased pressure drop is a result of horseshow vortex formation as flow approaches the stagnation region of the cylinder. As against this dimples increase convective heat transfer but do not increase the pressure drop considerably. Dimples cause turbulent mixing near the bottom surface of the channel in the regions downstream to their location leading to increased heat transfer rates in these areas. In order to get a reduced pressure drop at the expense of heat transfer rate, we have studied the effect of combined pin fin and dimple arrangements on the heat transfer and pressure drop. Heat transfer characteristics and the associated pressure penalty for five different configurations viz., pin fin, spherical dimple, pin fin with spherical dimple, pin fin with cylindrical dimple and pin fin with v-slot dimple have been studied. These configurations present in low aspect ratio channels are commonly seen in trailing internal cooling passages in gas turbines and compact thermo-electric generators. Pin fins extend all through the channel height while the dimples have a depth of 0.2 times the height of the channel. Wide range of Reynolds number from 8200 to 49500 are numerically investigated. Realizable k-epsilon model which solves Reynolds averaged Navier-stokes equations (RANS) was used for numerical simulations. Flow field characteristics were visualized in detailed in order to understand the effect of various features on local Nusselt number variations. It was seen that Nusselt number enhancement reduced with Reynolds number. Highest Nusselt number enhancement was seen for pin fin with v-slot dimple which was 3% higher than pin fin with cylindrical dimple , 28% higher than pin fin with spherical dimple , 39 % higher than pin fin and 178% higher than spherical dimple at Re = 8200. Highest pressure penalty was seen for pin fin with cylindrical

dimple and pin fin with spherical dimple configuration which was 15 % higher than pin fin with v-slot dimple at Re = 8200. Overall thermal-hydraulic performance was highest for pin fin with v-slot dimple and lowest for pin fin configuration. On comparing the performance factor based on the area enhancement due to the features, Pin fin with v-slot dimple performed better than other configurations.

NOMENCLATURE

D_h Hydraulic diameter [m]

D Pin fin diameter [m]

b Dimple print diameter [m]

δ Dimple depth [m]

S_1 Spanwise pin fin spacing [m]

S_2 Streamwise pin fin spacing [m]

S_3 Span-wise Pin Fin – Dimple Spacing [m]

f Friction factor

f_0 Friction factor for fully developed tube flow

h Heat transfer coefficient [W/m^2K]

k Thermal conductivity [W/mK]

L Channel Length [m]

L_p Length of pin fin [m]

Nu Nusselt number

Nu_0 Nusselt number from Dittus-Boelter equation

p Pressure [Pa]

Pr Prandtl number

q'' Heat flux [W/m^2]

Re Reynolds number ($u_{in}D_h/\nu$)

T Temperature [K]

T_{bulk} Bulk fluid temperature [K]

T_{in} Fluid temperature at inlet [K]

T_{wall} Wall temperature [K]

TKE	Turbulent kinetic energy [m^2/s^2]
TKE^*	Normalized turbulent kinetic energy (TKE/u_{in}^2)
u	Total fluid velocity [m/s]
u_{in}	Mean fluid velocity at inlet [m/s]
ϱ	Density (kg/m^3)
ν	Kinematic viscosity (m^2/s)
η	Thermal hydraulic performance factor

INTRODUCTION

As documented in the review paper by Arik and Bunker et al [1], gas turbines are mainly associated with turbulent flows while electronics cooling industries mainly have flow in laminar-turbulent transitional regime. They have also shown the need for better heat transfer technologies in electronics cooling industry which have been exploited to a great depth in gas turbines. Their literature review shows applicability of turbine heat transfer practices in electronics and heat exchanger industry. This has increased the interest in exploring already existing heat transfer technologies like rib turbulators, pin fins, dimples, lattice structures etc.

Dimple:

Due to the high heat transfer enhancement associated with rib turbulators, they were the main focus of research in olden days. This focus then shifted to dimples, as researchers sought for substitutes which provided better thermal – hydraulic performance. Dimples have been prime research interest since then. They have lower heat transfer enhancement compared to rib turbulators, but they also have lower pressure drop penalty associated with them. **Schukin** et al. [2] compared the heat transfer coefficients on a plate with single dimple in straight and diverging channels. They showed that the Nusselt number enhancements up to 125 % in comparison to smooth surface could be achieved. **Terekhov** et al [3] concluded that heat transfer enhancement inside the single hemispherical dimple was dependent on the increase in the surface area of cavity as well as flow oscillations around the dimple. A review by **Nagoga** et al. [4] gives a comprehensive understanding of effect of various geometrical parameters like dimple depth-to-diameter ratio, channel height-to-dimple diameter ratio,

and dimple spacing on heat transfer and pressure loss characteristics. Their study summarized that larger dimple depth yielded in higher heat transfer augmentations at the expense of high pressure losses. Closely spaced dimple arrays results in increased heat transfer. These increments in heat transfer in tightly spaced array came at a cost of high pressure loss and they observed that friction factor decreased with increasing Reynolds number. **Chyu** et al [5] studied hemispherical and tear drop dimples. These dimples showed heat transfer enhancements of 2 - 2.5 times that of smooth channel at a pressure penalty half of that found in case of protruding elements like pin fins and rib turbulators. This study was continued by **Zhou and Acharya** et al [6] where they investigated four different types of dimple configurations viz., square, triangle, circular and tear drop at Re = 21000. Experiments and numerical simulations showed satisfactory agreement and they concluded that tear drop shaped dimples performed the best out of the four configurations. The study by **Moon** et al [7] showed that the heat transfer and pressure loss remained fairly by variations in channel height to the dimple depth ratio. Flow structure inside and around the dimples was studied by **Lin** et al [8]. This study gave insight into the flow features and the corresponding heat transfer enhancement. The experimental investigations of **Mahmood** et al [9] focused on heat transfer using Infrared thermography to study the effect of air inlet stagnation temperature to local surface temperature and Reynolds number on the heat transfer measurements in dimples. Computational studies in stream wise –periodic channels were carried out by **Choudhury** et al [10] to understand in detail the heat transfer and flow characteristics in dimpled channels. Flow structures inside the dimples were presented by **Ligrani** et al [11] which helped in better understanding of the heat transfer characteristics. A computational work by **Isaev** et al. [12] showed the presence of counter rotating vortex pair in case of steady flow over a symmetrical dimple. Heat transfer enhancements even above 2 were noted by **Syred** et al [13] over a concave surface with single dimple. The geometry studied by **Zhou** et al [14] had dimples imprinted on the opposite walls and the experiments were carried out under stationary as well as rotating conditions. Enhancement factors about 2 were seen in these cases. Nusselt number enhancements between 0.5 – 2 inside the dimple and higher values along the dimple edges were reported by **Isaev** et al [15]. They also indicated the peak enhancement in the Nusselt number occurred along the downstream edge and the dimple edge in their case attained a value as high as 5. **Bunker** et al [16] conducted experiments for four different dimple configurations, viz. hemispherical sector dimple, inverted – truncated cones, shallow cylindrical pits, and a combination of cone and cylindrical pit in converging and diverging channels at three different Reynolds number. In case of a constant cross-section channel, hemispherical sector concavity array had heat transfer enhancement of 35 - 45 % and

pressure drop of 5% more than smooth surface. In converging channel, hemispherical sector and cone concavities showed equal heat transfer augmentation which was more than the cylindrical pit and cone-pit. In diverging channel, cone – pit, hemispherical and cone performed equally well. The authors carried out both experimental and computational investigation of heat transfer for four dimple configurations in a square passage at Re = 21000. They concluded that tear-drop shape provided highest heat and mass transfer. A counter rotating vortex pair was observed in the wake of triangular dimple while a single vortex roll was noticed in the wake for circular and teardrop geometries for a constant dimple depth of 3 mm in all configurations.

V-shaped dimples were investigated to a great extent by **Wright** et al [17, 18, 19], where they studied v-shaped dimples in a rectangular channel of aspect ratio 3:1. They also investigated the effect of inline and staggered array combination and dimple depth ($\delta/D = 0.15 - 0.3$) of v-shaped dimples on heat transfer characteristics and pressure penalty incurred. Results were taken on wide range of Reynolds number varying from 10,000 to 40,000. They concluded that the v-shaped dimples performed similar to spherical type of dimples at low Reynolds number. However, for Reynolds number ranging between 10,000 to 40,000, stronger secondary flows were seen to develop from the concavities which further enhanced the heat transfer downstream of the dimpled surfaces. These shaped proved beneficial as they marginally increased the pressure drop at higher Reynolds number , thus giving high thermal performance values even at high Reynolds numbers. They saw that the average heat transfer coefficient remained fairly unaffected by the Reynolds number in the range of the dimple depths considered, however, the difference between maximum and minimum heat transfer coefficient reduced with decreasing dimple depths. In case of inline configuration, the Nusselt number increased with increasing Reynolds number, however in case of staggered configuration, a decreasing trend for Nusselt number was seen with increase in Reynolds number.

Pin fin:

A lot of research was carried out to characterize the flow pattern and heat transfer behavior of pin fins. Long pins were mostly researched for tube exchanger applications by **Zukansas** et al**.** [20] et al. Due to trailing edge passage being very narrow there were limitations with respect to size and manufacturing so, short pin fins were cast into the coolant passage. Therefore, in turbines generally pins of size lesser $0.5< H/D <4$ where H is the height of the pin fin and d is the diameter of the pin fin were implemented. [21]

Vanfossen et al. [22] investigated the heat transfer characteristics if short pin fins. They studied a wide range of Re – 300 and nearly 60000. Heat transfer coefficients for short pin fin were found to be lower than that for long pins. Heat transfer coefficient on pin surface was about 35% higher than on the bottom surface of channel. Also passages with pin fins showed considerably higher heat transfer coefficients than plain channel with no pins. This study indicated a need to develop better understanding of the dependence of length of short pin fin on heat transfer. This relationship was studied by **Bringham** and **Vanfossen** et al [23]. They concluded that pin length to diameter ratio was a dominant factor in array averaged heat transfer coefficients for short pin fins (endwall included). Also in case of pin fin to diameter ratio (Lp/D) less than 2 , Nu was a function of Re alone while for pin fin to diameter ratio (Lp/D) greater than 2 , Nu was a function of Length to diameter ratio as well as Re. **Simoneau** and **Vanfossen** et al [24]. described the effects of changing the number of pin fin rows. Streamline turbulence intensities and pin surface heat transfer coefficients were measured as the test gas temperature varied between 260 K and 290 K.

Sparrow and **Ramsey** et al. [25] studied the effect of inline and staggered pin fin configurations. The study concluded that in-line array transferred more heat at fixed pumping and surface area. Staggered array however minimized the surface area at a fixed heat load and flow rate. **Sparrow and Ramsey** et al [26] investigated behavior of pin fin with a clearance space between the free end of the pin fin and the other wall. The heat transfer coefficients showed variations only in initial few rows and a constant value of heat transfer coefficient was attained after fourth row attained. Also, it was found that the heat transfer coefficient value seen in fully developed flow region was not affected by cylinder height and heat transfer coefficient increased moderately as the height increased.

Metzger et al. [27, 28] investigated the heat transfer and pressure loss in channels with both endwall and pin fins being thermally active. Staggered configuration of pin fin was chosen in this study. Maximum local heat transfer enhancement was seen close to third or fourth row which indicated to highest level of mixing and increased turbulence. A patterned flow was developed in the successive rows. Short pin fins were studied to understand the effect of stream wise spacing or compactness of array while maintaining uniform lateral spacing. It was seen that heat transfer enhancements showed a strong dependence on stream wise spacing. Average heat transfer enhancements ranging from 50 – 100 % were seen closely packed configurations. From his study, **Chyu** et al [29] stated that 10- 20 % higher heat transfer enhancement were seen on pin fins than that on endwall. They made these conclusion based on experimental results for a wide range of Reynolds number.

Thole et al [30, 31, 32] did a detailed study of pin fins in short aspect ratio channels in order to explore effects of array arrangement on the overall heat transfer enhancement. One of the study [30], effect of streamwise and spanwise spacing on heat transfer characteristics of the channel was investigated. It was seen that spanwise pin spacing affected array pressure loss greater that the effect of streamwise spacing, but, streamwise spacing had a larger effect than spanwise spacing on array heat transfer. They [31] also showed that downstream vortex shredding in pin fin wake region was seen to get suppressed and asymmetric wakes were created as the spanwise spacing was decreased from 3 to 1.5. It was seen that S/D >= 2 was beneficial for heat transfer enhancement. Vortex shredding in the first few rows reduced as the streamwise spacing was decreased. For X/D > 2.60, Pin fin heat transfer showed an increase on the trailing side but the array average heat transfer reduced in downstream rows. In one of the other study [32] on short pin fins, they found that the heat transfer was highest for smallest spanwise spacing (S/D = 2) and lowest Reynolds number.

Relative contribution of pin fin and endwall was investigated by **Metzger** et al [33] .In their study of effect of orientation of circular and oblong pin fins on endwall heat transfer and pressure loss , higher heat transfer values were seen for oblong pin fins at the expense of increased pressure penalty. Inline and staggered arrangements of square and diamond pin fins were analyzed by **Chyu** et al [34]. He concluded that cubic pin fins performed better than diamond pin fins. Higher heat transfer enhancements at lower pressure drop for cubic pin fins was found to be comparable to diamond pin fin case. Recently, **Kirsch and Thole** [35] compared pin fin heat transfer due to oblong and cylindrical pin fins. Height to diameter ratio was maintained to unity and the streamwise and spanwise spacing was varied between 2 to 3 diameters. Cylindrical pin fin surfaces yielded 30 -35% higher heat transfer coefficient on the pin fin surface than oblong pin fin.

Dimple with Pin fin configuration:

Taslim et al [36] modified the surface projection features to come up with conical bumps or radial turbulators. The enhanced heat transfer in these cases were mainly due to the increased surface area of the protruded surface geometries. A combination of dimples on one wall and protrusion on other wall were investigated by **Mahmood** et al[37]. **Bunker** et al [38] came up with mixed enhancement mode geometries in their study where short pin fins were combined with turbulators and concavities. High heat transfer enhancement factors up to 3.3 were witnessed in such geometries for Re ranging from 2500 to 10000. **Rao** et al [39,40,41,42] first implemented pin fins and spherical

dimpled surfaces together in their study. The experimental results were compared with numerical simulation data and a good agreement of error within 10% was achieved. The results show that pin fin with dimple channel resulted in higher overall endwall heat transfer enhancements as compared to pin fins only. They attributed this increase to the enhanced turbulent mixing experienced in case of pin with dimple channel.

Main objective of current study is to achieve heat transfer enhancement in short pin-finned channels. Hence, concavities in the form of spherical, cylindrical and v-slot dimple are added to the pin fin configuration. In current study, numerical simulations are carried out for the model similar to that in the **Metzger** et al's study [27,28,33]. Five different configurations have been studied which include pin fins, spherical dimples, pin fin with spherical dimple , pin fin with cylindrical dimple and pin fin with v-slot dimple. Flow field characteristics and Nusselt number distributions are studied in detail for Reynolds number ranging from 8200 to 49,500. In order to understand the effect of features on pressure penalty, friction factor has been calculated for all the configurations and at all Reynolds number. In order to validate the results of the simulations, the overall Nusselt number average data has been compared with empirical correlations from literature.

NUMERICAL PROCEDURE

This section discusses the description of computational geometry taken under consideration for Current Study.

Description of Computational Geometry

Three dimple geometries in conjunction with pin fins were studied and heat transfer coefficients and flow characteristics are reported. Numerical simulations were carried out on following configurations: - pin fin, spherical dimple, pin fin with cylindrical dimple, pin fin with v-slot dimples. All features in above mentioned configurations were axisymmetric. Heat transfer variations were analyzed on bottom wall of wide-aspect ratio channel across 10 rows of stream-wise staggered array and 5 rows of span-wise array of pin fins. Span-wise spacing-to-diameter ratio (S_1/D) of 2.5 mm and stream-wise spacing – to – diameter (S_2/D) ratio of 2.5 mm similar to one used in **Metzger** et al.'s [27, 28, 33] study was investigated. Definitions of all parameters are shown in Fig. [1]. Table [1]

provides details of geometrical parameters of all configurations. The test section had a width of 12.4 cm, height of 1 cm and length 24.0 cm resulting in a width–to-height ratio of 12.4:1. Thus the hydraulic diameter of the channel is 1.850 cm. The pin fin extended all through the height of the channel, thus height of the channel-to- pin fin diameter ratio was 1. Same geometric configuration was retained for all types of plates. Dimple print diameter was taken to be 10 mm, dimple depth and diameter were 2 mm (0.2 *D*) and 14.5 mm respectively. Thus, the ratio of channel to dimple print diameter,H/D, was 1 and ratio of dimple depth to dimple print diameter was δ/D is 0.3.Spanwise pin fin – dimple spacing (S_3/D) is 1.25. Similar geometry for pin fin / pin fin dimple plate was seen in **Rao** et al study [39, 40, 41, 42]. Same dimple print diameter was maintained in all configurations. Bottom wall surface area comparison data shown in Table [2] was later used to calculated enhancement in overall heat transfer. A duct length of 5 D_h was added after outlet so as to avoid reverse flow and effect of outlet boundary condition on the flow field close to the outlet.

Table 1: Geometrical Parameters

Length of channel	L	124 mm
Height of channel	H	10 mm
Hydraulic Diameter	D_h	18.50
Pin Fin Diameter	D	10 mm
Dimple Print Diameter	h	10 mm
Dimple Depth	δ	2 mm
Span-wise Pin Fin Spacing	S_1	2.5 mm
Stream-wise Pin Fin Spacing	S_2	2.5 mm
Span-wise Pin Fin – Dimple Spacing	S_3	1.25 mm

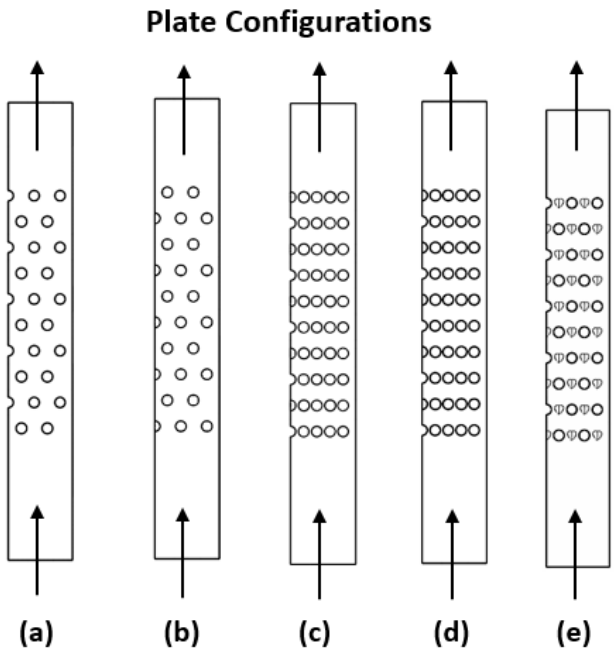

Figure [1]: Top view of computational geometries of five different configurations: (a) pin fin, (b) spherical dimple, (c) pin fin with cylindrical dimple, (d) pin fin with spherical dimple, (e) pin fin with v-slot dimple

Table 2: Area Ratio for all configurations

Confg.	A_p/A_{wet}	A_d/A_{wet}	A_e/A_{wet}	Diagram
Pin Fin	0.3515	-	0.6485	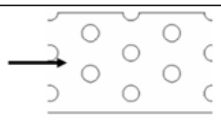 $S_1/D = 2.5$ $S_2/D = 2.5$ $H/D = 1$ $h/D = 0.2$ $\delta/D = 0.3$
Spherical Dimple	-	0.1352	0.8648	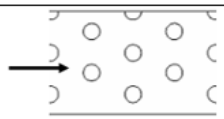 $S_1/D = 2.5$ $S_2/D = 2.5$ $H/D = 1$ $h/D = 0.2$ $\delta/D = 0.3$
Pin Fin + Spherical Dimple	0.3466	0.1005	0.5529	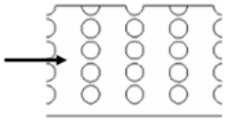 $S_1/D = 2.5$ $S_2/D = 2.5$ $H/D = 1$ $h/D = 0.2$ $\delta/D = 0.3$ $S_3/D = 1.25$
Pin Fin + Cylindrical Dimple	0.3194	0.1437	0.5095	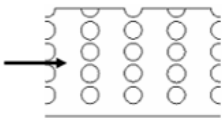 $S_1/D = 2.5$ $S_2/D = 2.5$ $H/D = 1$ $h/D = 0.2$ $\delta/D = 0.3$ $S_3/D = 1.25$
Pin Fin + V-slot Dimple	0.3488	0.0873	0.5631	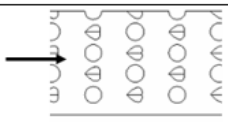 $S_1/D = 2.5$ $S_2/D = 2.5$ $H/D = 1$ $h/D = 0.2$ $\delta/D = 0.3$ $S_3/D = 1.25$

Table 3: Test Matrix

Configuration	Reynolds Number
Pin Fin	8500 , 18600 , 36700 , 49500
Spherical Dimple	
Pin Fin + Spherical Dimple	
Pin Fin + Cylindrical Dimple	
Pin Fin + V-slot Dimple	

Numerical Simulation

This section provided details of the computational grid and boundary conditions chosen for this study.

Computational Grid and Boundary Conditions

Only one half of the computational geometry was taken into account during simulations so as to save computational time as solving three dimensional Navier-Stokes equations and the energy equation is computationally expensive. The geometry is symmetric about the center plane and hence symmetry boundary condition was employed. The bottom wall of the channel was heated, while the top and the side walls were declared adiabatic. Additional channel length was provided downstream of the last feature row to avoid back pressure effects on heat transfer results in the region of interest.

Fig [2] summarizes the boundary conditions for the computational domain. For computational purpose, air is considered as incompressible ($0.02<Ma<0.1$). A constant velocity is provided at the channel inlet depending on the channel Reynolds number ($Re_{D_h} = 8200 , 18700 , 36700 , 49500$). Turbulence intensity and length scale at inlet were specified to be 5% and 10% of the channel hydraulic diameter, respectively. Outlet of the channel was set at zero static gage pressure. A constant and uniform heat flux of 5 $kW/m^2$was provided on the bottom wall, including dimple surface and sidewalls of the pin fins. This value was chosen to maintain a difference of about 20 ℃ between inlet and outlet temperature so as to avoid uncertainties in computational results. Sidewalls of the channel were adiabatic. All the surfaces were treated as no-slip boundaries.

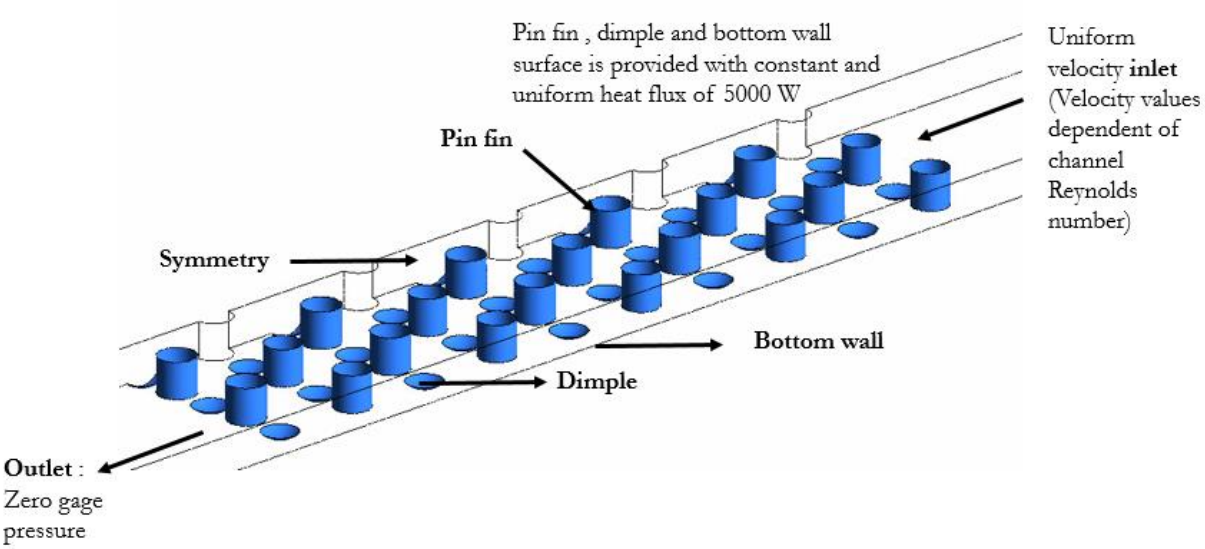

Figure [2]: Boundary conditions for numerical study

Grid Generation

Unstructured mesh was generated using ANSYS CFX meshing software. The mesh consisted of a combination of tetrahedral, pyramidal and prismatic elements. Figure [3] shows the details of the mesh generated for the current study. A mesh grid near the walls consisted of 10 – 15 layers with a growth rate of 1.2 in order to accurately capture the boundary layer flow interactions. Very fine mesh grid was set up in and around dimples and around pin fin sidewalls, which were the regions of prime importance and complicated flow physics. A yplus of 1 – 3 was maintained at fluid walls. A yplus in the above mentioned range was necessary for proper functionality of near wall equation used in this study.

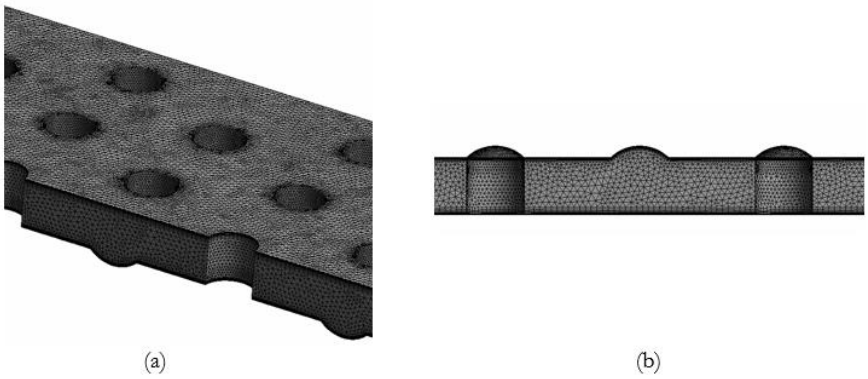

Figure [3]: (a) Numerical grid (b) Cut-section view of the mesh

Computational Model

ANSYS Fluent 14.5 was used to carry out numerical simulations. Steady, incompressible Reynold's-averaged Navier-Stokes (RANS) equations were solved using the finite-volume based solver. Time-averaged values for velocities and other scalar quantities were obtained from RANS equations. Realizable k-epsilon (RKE) turbulence model was able to resolve flows with complex secondary circulations located close to the surface in dimpled channels as seen by **Ligrani** et al [43]. Also, **Xie** et al [44] investigated that this model was able to predict flow swirling and separation seen in pin fin channel. A study conducted by **Rao** et al [42] on pin fin with spherical dimple configurations suggested that RKE suited best for such applications having compound features. Enhanced wall treatment function was enabled during simulations so as to accurately predict the wall heat transfer. FLUENT used finite volume method for discretization of governing equations viz. continuity, Navier-Stokes, energy equation, etc. Second-order upwind scheme was used for spatial discretization for scalar transport equations for high order accuracy from numerical simulations. Simple-Implicit Pressure-linked equations based pressure-velocity solver was employed in current study. Minimum convergence criterion was 10^{-5} for continuity, x-velocity, y-velocity, z-velocity and turbulence quantities while for energy equation it was kept lower to 10^{-8}. Temperature monitors at various locations on the domain were continuously monitored to check convergence.

DATA REDUCTION

In order to compare the overall performance of the configurations, average heat transfer coefficients and pressure drop across the channel are calculated for all the configurations. Also, flow field characteristics and their effect on local heat transfer enhancement are understood by identifying secondary flow patterns and turbulence produced.

Steady –state heat transfer coefficient was calculated from,

$$h = \frac{q"}{(T_{wall,x} - T_{bulk,x})} \quad \text{.....................................(1)}$$

where, $q"$ is the heat flux applied on the bottom wall , T_{wall} is the local wall temperatures and T_{bulk} is local bulk temperature. This temperature was calculated by averaging the bulk temperature over planes at several streamwise locations and then fitting a curve to approximate the trend of bulk temperature variation. This linear interpolation method is validated with experiments done by Metzger et al.[27,28,33] for pin fin configuration. A close agreement is observed between the heat transfer coefficient from numerical simulations in this study and that form Metzger et al.[27,28,33] experiments, and hence linear interpolation method was used for other configurations as well.

Nusselt number values are obtained from following formula,

$$Nu = \frac{hD_h}{k} \quad \text{..(2)}$$

where, h is the local heat transfer coefficient , D_h is the hydraulic diameter of the channel and k is the thermal conductivity of fluid which is air in this case.

In order to estimate the local enhancement of Nu over the baseline case of smooth channel, local Nu values were normalized using fully developed, turbulent flow in smooth tube as provided by Dittus-Boelter correlation for heating at same Reynold's number:

$$\frac{Nu}{Nu_o} = \frac{hD_h}{k_{air}(0.023Re^{0.8}Pr^{0.4})} \quad \text{.....................................(3)}$$

Properties of air were chosen based on the bulk temperature of the air with a Prandtl number of 0.76. Due to the added concavity to the bottom wall, increased pressure drop was caused as compared to the baseline case of smooth channel. Friction factor gives an indication of this increase in pressure drop and can be calculated using following formula:

$$f = \frac{2\ \Delta P}{4\ \rho_{air} v_{air}^2 \frac{L}{D_h}} \quad \text{...(4)}$$

where, ΔP is the pressure drop across the channel , L is the length of the channel and D_h is the hydraulic diameter.

First law of Blasius, Fanning friction factor was used for normalizing friction factor , which is given be ,

$$f_0 = 0.079Re^{-0.25}$$

The overall thermal-hydraulic performance factor can be estimated by taking into account the heat transfer enhancement as well as the pressure drop using the following formula,

$$\eta = \frac{\frac{Nu}{Nu_o}}{\left(\frac{f}{f_o}\right)^{1/3}} \qquad \text{.....(5)}$$

The configurations considered in this study increase the wetted surface area significantly along with low or moderate increase in pressure drop. The enhancement in heat transfer can be attributed to both fluid dynamics as well as increased area. In order to consider the increase in wetted surface area along with the increase in heat transfer coefficient, Bunker et al compared the product of heat transfer coefficient 'h' and wetted surface area 'A_{wetted}' called 'hA' . They also calculated performance factor base on this product for better understanding of individual contributions of fluid dynamics and surface area increment.

$$PF = \frac{\frac{hA}{(hA)_o}}{\left(\frac{f}{f_o}\right)^{1/3}} \qquad \text{.....(6)}$$

where, $(hA)_o$ is the product evaluated for baseline case of smooth channel.

In both overall thermal-hydraulic performance and performance factor, more weightage is given to the heat transfer enhancement rather than pressure losses which scale by a factor of 0.33.

RESULTS AND DISCUSSION

In this study only fluid domain has been taken into consideration. It can interpreted that simulating only the fluid domain and applying constant and uniform heat flux on all the walls is similar to conducting experiments employing a material of extremely high conductivity where the efficiency of the features is 1.[45] This section, discusses the flow field characteristic and the Nusselt number variation in all the configurations. Contours for normalized velocity, temperature and turbulent kinetic energy have been plotted on plane 1 given in Fig. [6]. Plane 1 lies at a distance of 4% of D_h from the bottom surface.

Grid Independence

A grid independence was carried out for the pin fin configuration to achieve a solution which is independent of the mesh grid. Three mesh levels were investigated, the coarsest having 4.8 million elements and the finest having 10.3 million elements. The variation of Nu and friction factor with mesh level is given in Fig. [4]. For grid independence study, globally averaged Nusselt number and overall friction factor were compared. The average Nusselt number value for medium mesh level showed a difference of less than 0.1 % as compared to the finer mesh level. Qualitative agreement between the trends for friction factor was seen between numerical simulation results and Metzger et al's experimental results. Considering computational time and accuracy, medium mesh level of – million elements was chosen for further computations.

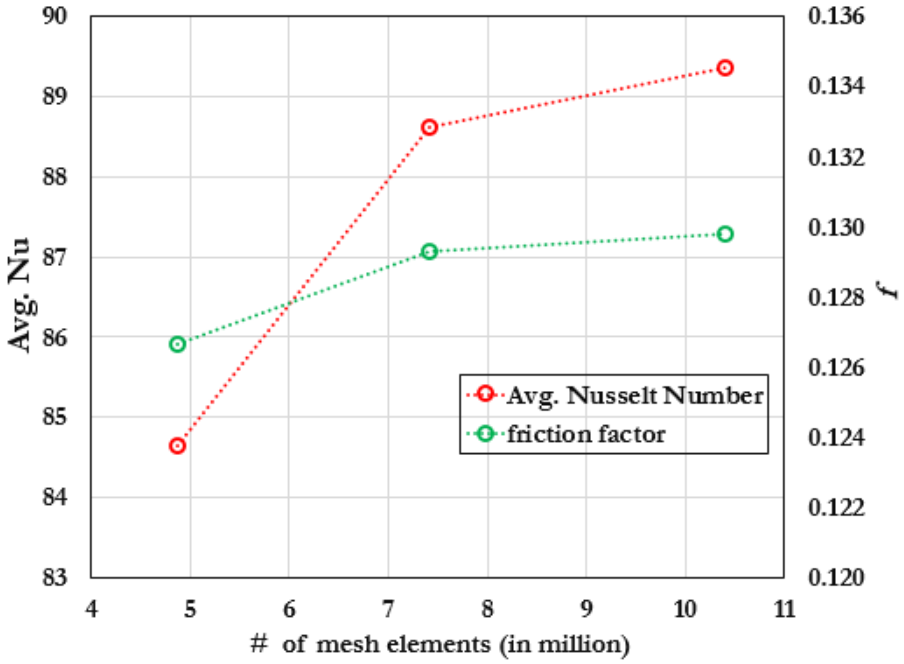

Figure [4]: Overall average Nusselt number and friction factor variation for different grid sizes

Validation of Numerical Results

In order to validate the numerical results, average Nusselt number from CFD simulations of pin-fin configuration were compared with Metzger et al' empirical correlations. The equation relating Nusselt number to Reynolds number in pin fin case of S/D = 2.5 and H/D = 1 , a configuration studied by Metzger et al gives $Nu = 0.08\, Re^{0.728} Pr^{0.4}$ .The objective was to determine the degree of accuracy to which the computationally obtained Nusselt number values can be predicted and whether the heat transfer characteristics are well represented.

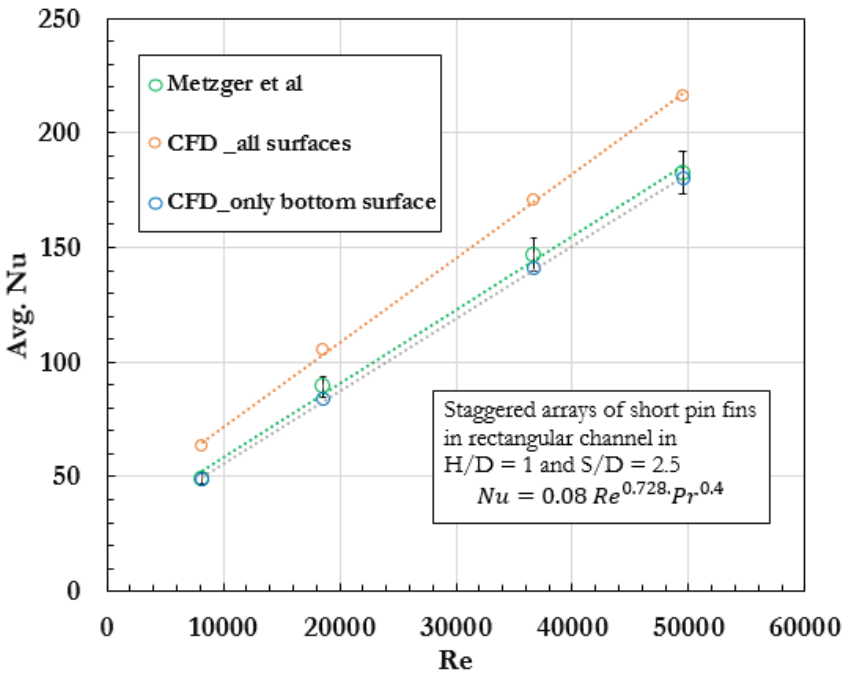

Figure [5]: Comparison of average Nusselt number

Figure [5] shows the trend line for Metzger et al.'s correlations and values for average Nusselt number for test plate obtained from simulations. Their study considered only the bottom surface without taking into consideration the pin fin surface while calculating average Nu values, hence a similar practice has been adopted in order to develop the co-relation in this study. The experiments conducted in their study used pin fins made out of balsa wood and hence were adiabatic. Another study [46] by them highlighted that conducting and non-conducting pin fin surfaces did not have a significant effect on the average Nu values. Hence, we can safely compare the results from simulations in this study with Meztger et al's empirical equation. A close agreement was seen in the results form numerical simulations and empirical correlation with an error of less than 5%. It could thus be concluded that the numerical simulations predicted the heat transfer well and could be used in deriving the average Nusselt number for various configurations.

Flow Field Development

Normalized velocity superimposed with velocity vectors has been plotted in Fig [6]. The trademark characteristic of pin fins denoted by stagnation region on the wall of the pin fin facing the flow and wake region extending few pin fin diameters on the opposite wall of pin fin have been well

captured by the simulations. Large wake region was observed in the case of pin fin configuration, where the flow was not interrupted by secondary flow from dimples. Short wake regions were seen in pin fin and dimple configurations.

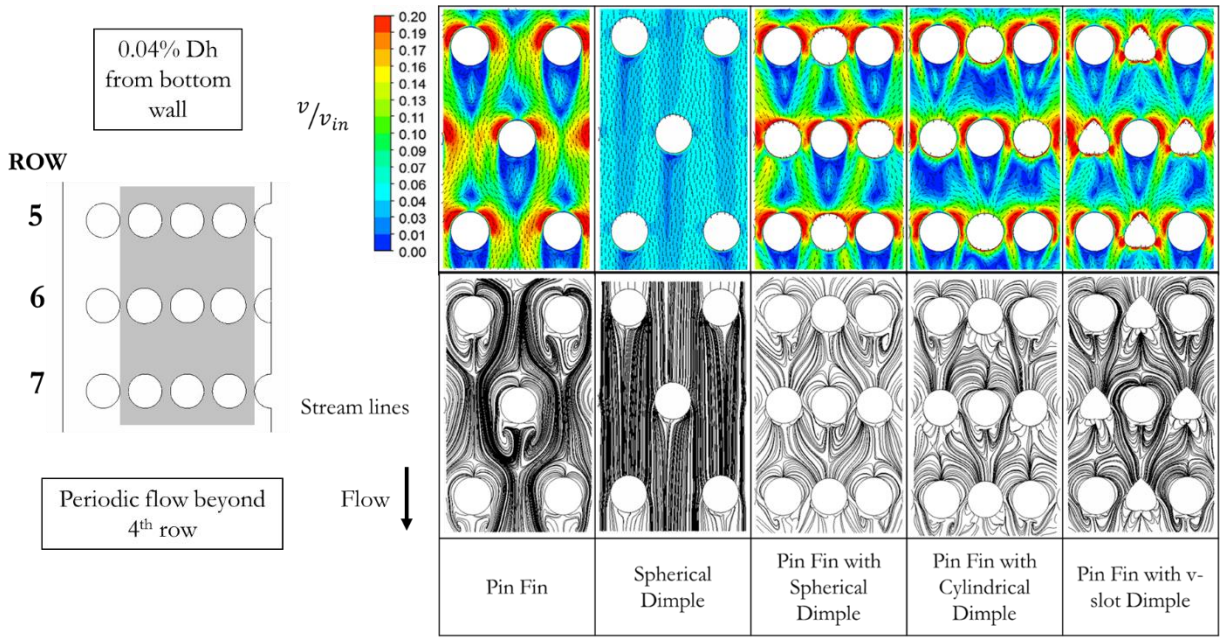

Figure [6]: Normalized velocity and streamlines plotted on a plane close to vectors close to bottom wall @ Re = 36700

The secondary flows from the dimples affect the extent of the wake region. As against the pin fin configuration, the regions immediately downstream of the dimple had higher velocities. Secondary flow ejecting out of the dimple results in large turbulence near the edge of the dimples. Some of the flow features peculiar to pin fin and dimple were retained in the pin fin with dimple configurations. As seen in the pin fin configuration, regions of large velocities which are present in the region between the pins were fewer in pin fin with dimple configurations. However, like dimple configurations, regions of lower velocities were increased in the compound feature configurations.

Wake region of pin fins are mainly associated with large recirculation. As expected from velocity contours, the wake regions should denote higher bulk temperature values as compared to the rest of the bottom wall. This is seen in Fig. [7]. Similarly high turbulence is seen along the edges and downstream of dimples caused by the mixing of the secondary flow into the primary flow. These regions of high turbulence have high heat dissipation levels. This corresponds to the low temperature regions seen downstream and near the dimple edges.

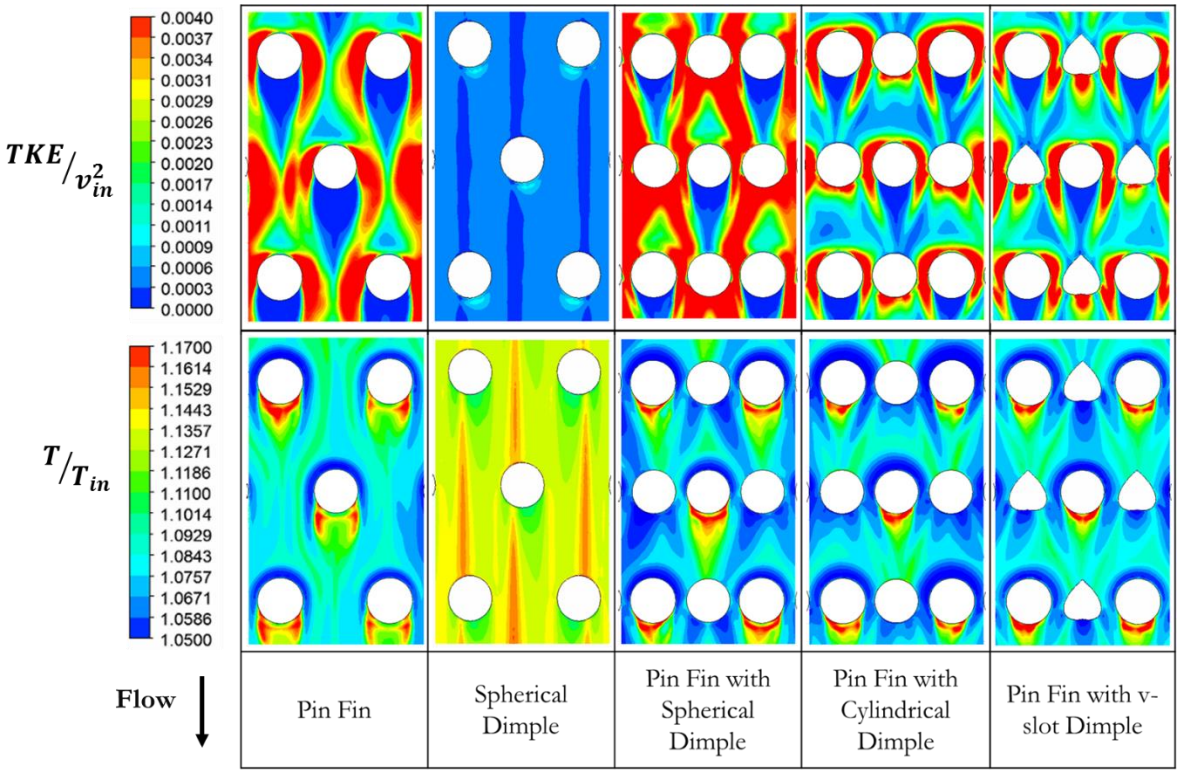

Figure [7]: Normalized turbulent kinetic energy and temperature plotted on a plane close to vectors close to bottom wall @ Re = 36700

Figure [7] shows the normalized turbulent kinetic energy (TKE) and temperature contours (for plane shown in Fig. [6]) for all four configurations at Reynolds number of 36700. The TKE contours helps in understanding the heat transfer characteristics of different configurations since the mixing caused by turbulence contributes significantly to the heat dissipation from the surface. In general, higher turbulent kinetic energy corresponds to higher heat transfer rate. The region downstream of the dimples show high turbulence rates. This is more pronounced in case of pin fin with cylindrical dimples and pin fin with v-slot configurations.

Flow Structures in Individual Configurations

In Figs. [9, 11, 13, 15, 17], velocity magnitudes have been normalized with average velocity at the inlet of the channel and turbulence kinetic energy with square of average inlet velocity. Normalized

turbulent kinetic energy plots were superimposed with tangential component of velocity vectors. In Figs. [10, 12, 14, 16, 18], normalized temperature and streamline shave been plotted. In all the Figs. [9-18] it should be noted that the flow is coming out of the page (viewed from the outlet side). Five planes have been considered for the study. The location of these planes has been marked in Fig [7]. Plane 1 is the plane located at the leading edge of the dimple. Plane 2 is located midway between the center of the dimple and the leading edge. Plane 3 corresponds to the center of the dimple. Plane 4 is midway between center of the dimple and the downstream edge of the dimple. Plane 5 corresponds to the downstream edge of the dimple row. All the contours have been plotted for Re = 36700.

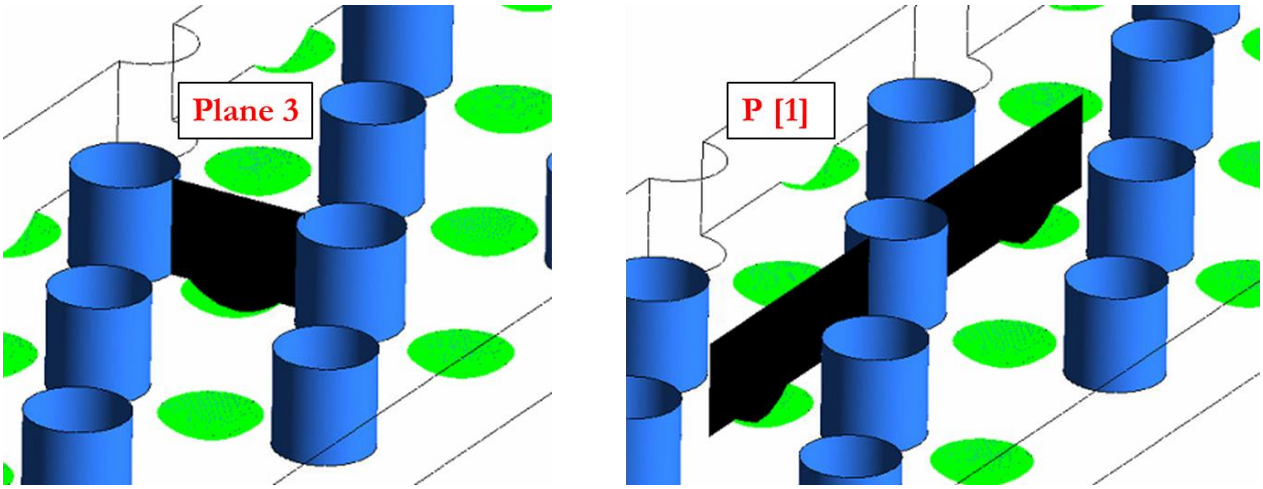

Figure [8]: Location of Plane 3 and P[1]

Pin Fin:

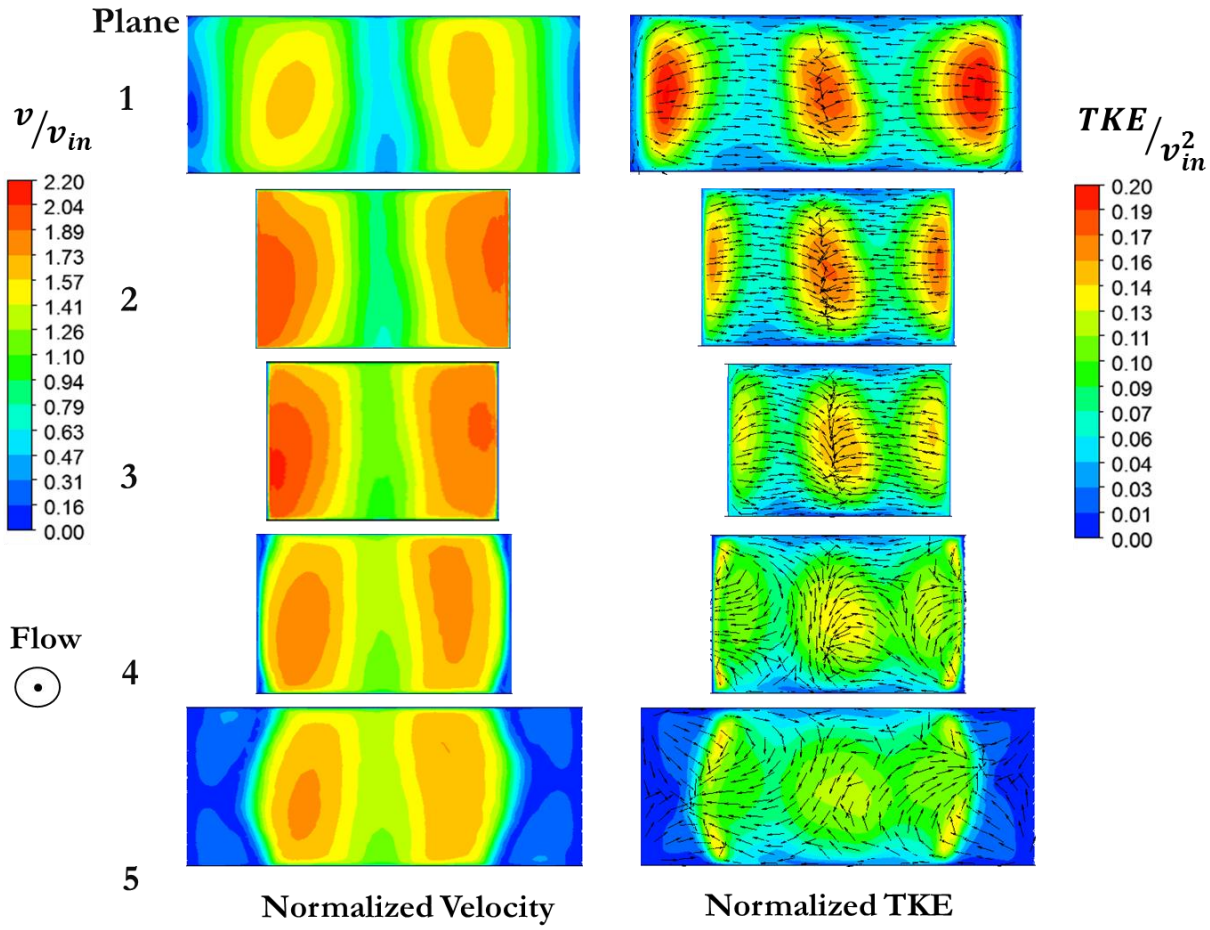

Figure [9]: Normalized velocity and turbulent kinetic energy superimposed with tangential velocity vectors for pin fin configuration @ Re = 36700

In Fig. [9], it can be seen in the velocity plot of plane 1 that as the fluid starts approaching the pin fin, slight disturbance is created. Large crossflow is seen in this region. The side walls of plane 1 are slightly away from the stagnation region. As the flow starts approaching narrow region at center of the plane (between pin fins), it experiences high mixing which is significant from the higher turbulence levels in this region. The fluid passing through the narrow gap picks up speed which is evident from the high velocity values in plane 2 -4. As the fluid pass out of the narrow gap, it suddenly expands into a wider cap between the two rows and hence low velocity values are seen in the along the side walls of the pin fin of the plane 5 which mainly represent the wake region. These regions of low velocity denote separation from the wall. Due to the turbulence cause by the fluid separating close to the wake region, higher velocity and TKE values are seen in plane 5 close to the center where streams separating from neighboring walls interact. From Fig. [10], it can be seen that regions of high turbulence correctly

signify low temperature regions, also higher temperature values are seen in the wake region having flow recirculation.

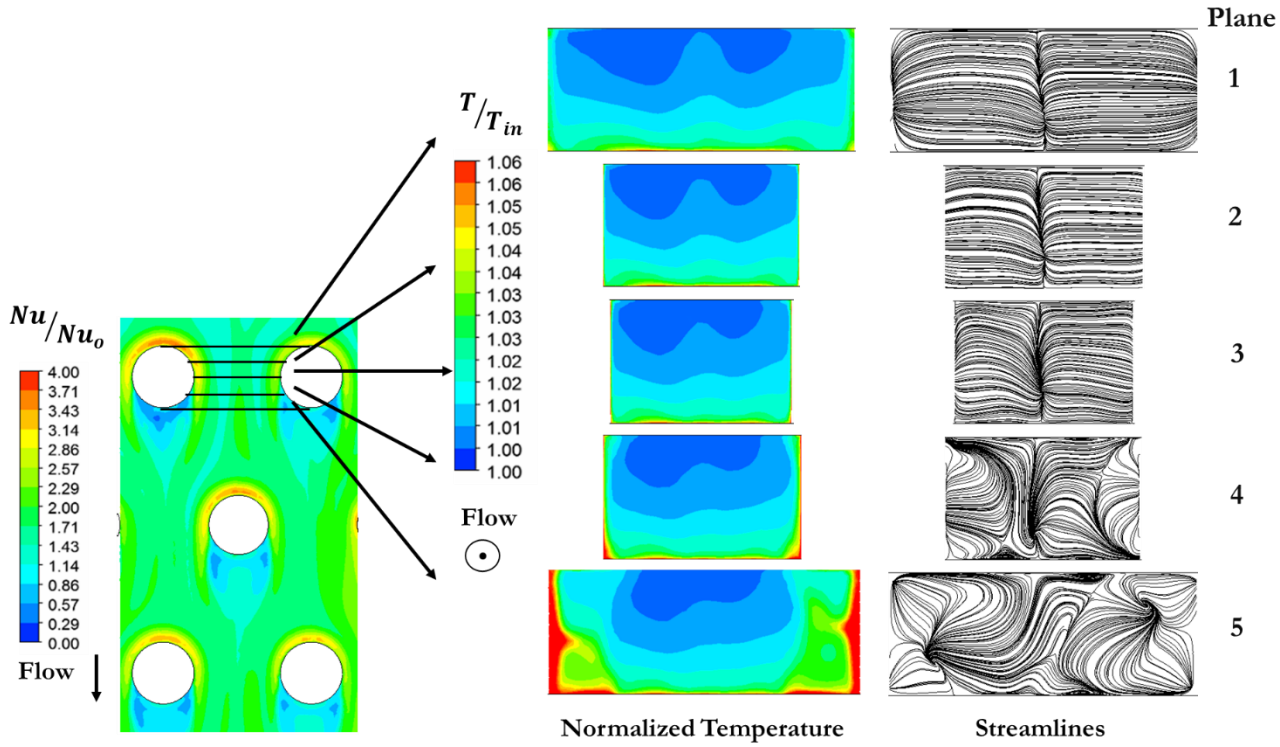

Figure [10]: Normalized Temperature and streamlines for pin fin configuration @ Re = 36700

Spherical Dimple:

Figure [11] shows the flow field for a dimple feature. As the flow encountered a dimple structure, minor disturbances as seen arising close to the wall. As seen in all the planes, rotating flow structures were seen on the two ends of the planes which were mainly similar to vortex rolls propagating from the earlier row. As the fluid passed through the dimple, slight mixing takes place near plane 2. This mixing results in recirculation close to the wall as seen in plane 3 inside the dimple concavity. Regions of low local velocities were encountered close to the wall in plane 1 -3. As fluid approaches plane 4 and 5, strong ejections of secondary flow emerging from downstream edge of the dimples can be seen. Previous rows had more pronounced effect on the up wash regions where they continue to entrain coolant near the surface and lifting it up from the core of the flow.

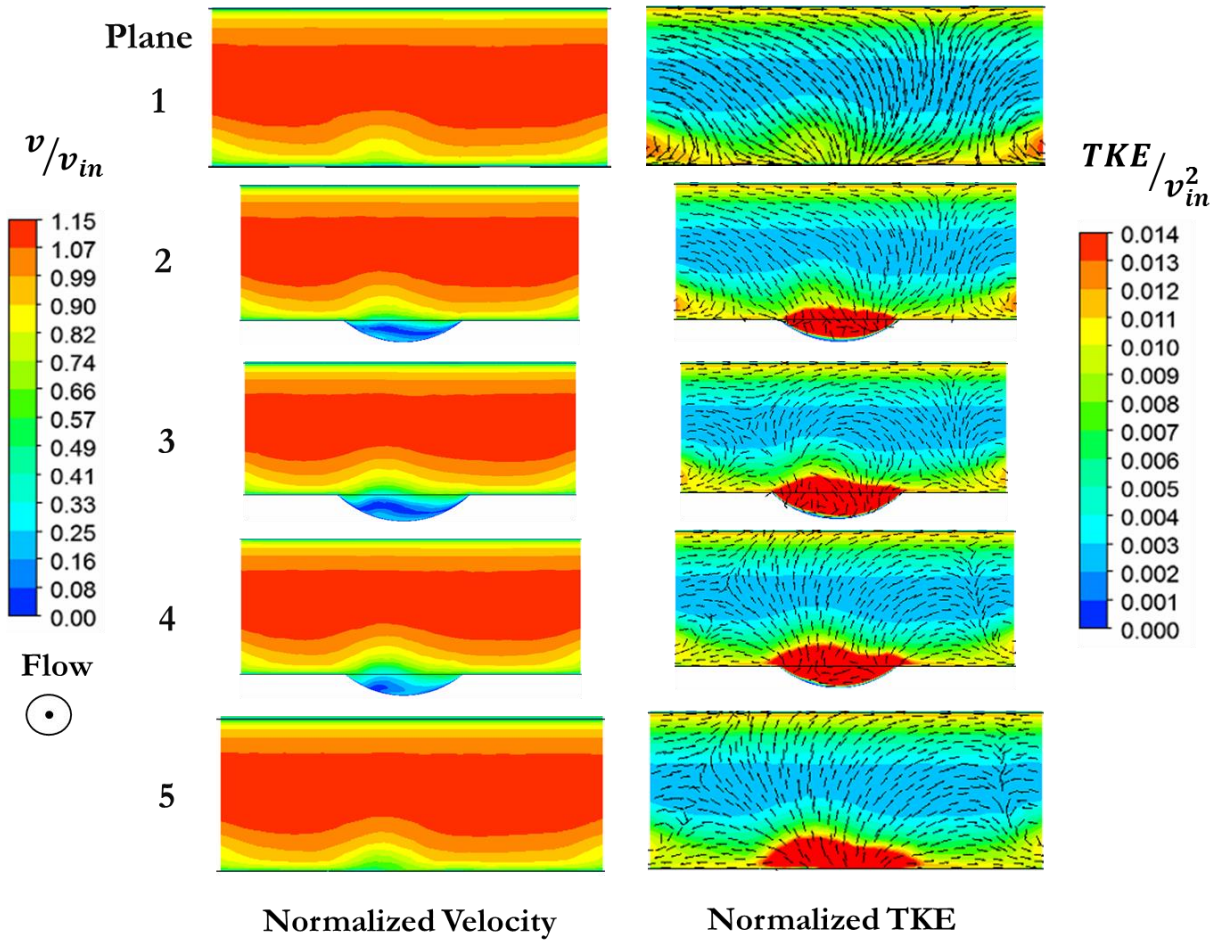

Figure [11]: Normalized velocity and turbulent kinetic energy superimposed with tangential velocity vectors for spherical dimple configuration @ Re = 36700

Figure 12, shows the temperature distribution close the wall in dimpled channel. The regions inside the dimple have high temperature due to the flow recirculation and hence denote low heat dissipation inside the dimples. These regions of flow recirculation die down towards the downstream of the dimple.

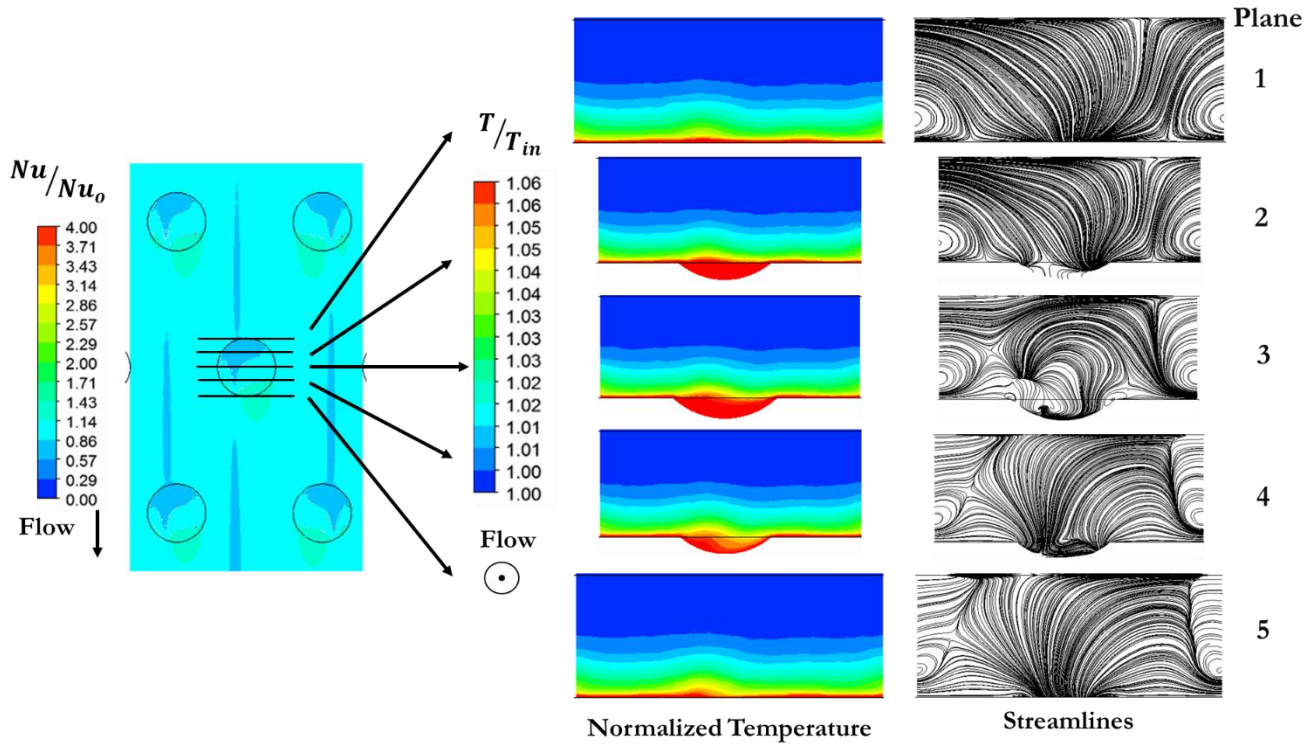

Figure [12]: Normalized Temperature and streamlines for spherical dimple configuration @ Re = 36700

Pin fin + spherical Dimple:

Similar characteristics as those in case of dimple and pin fin configurations, were seen in case of pin fin with dimple configurations in Figs. [13-16]. As the flow approached the dimple or the narrow gap between the pin fins, regions of strong turbulence were seen in the central portions of the planes which showed the dominance of the pin fin structures in these regions as it had a trend similar to that seen in Fig. [9].

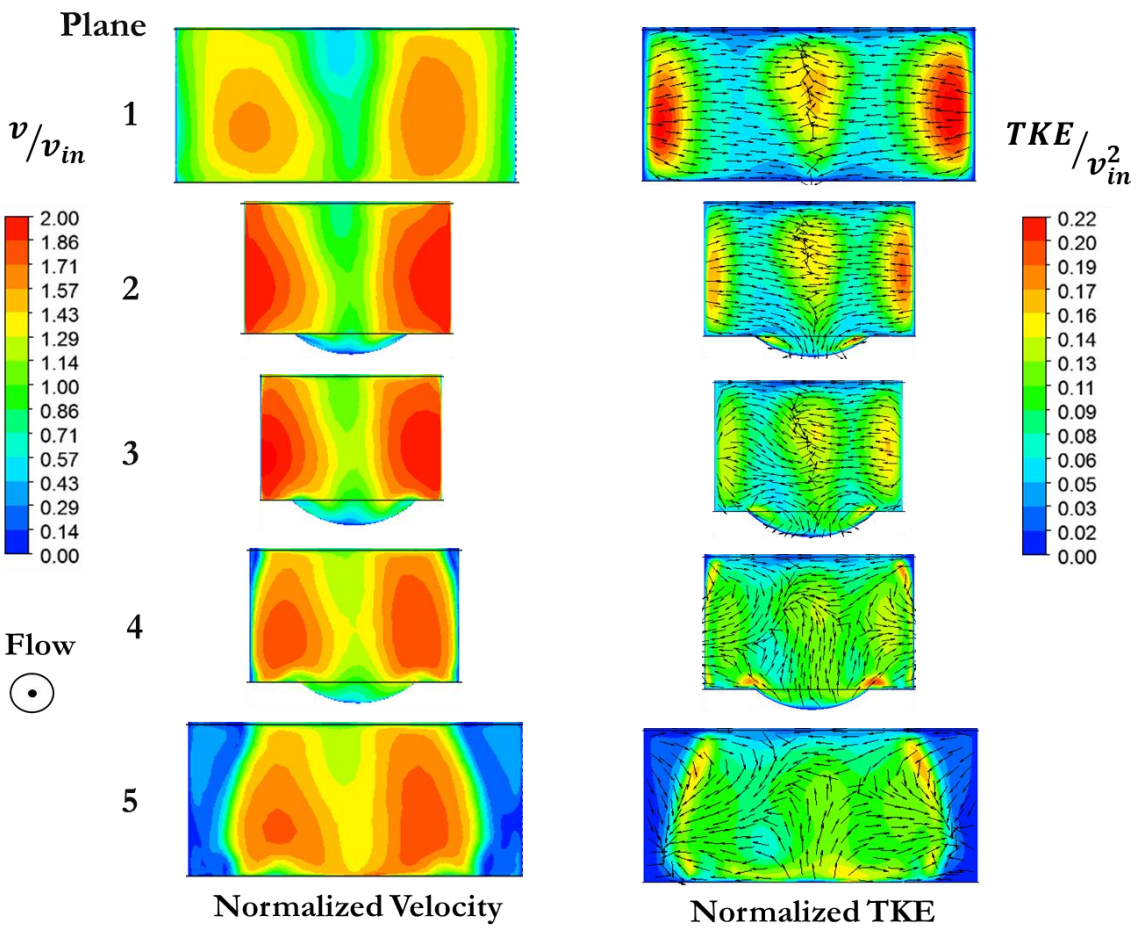

Figure [13]: Normalized velocity and turbulent kinetic energy superimposed with tangential velocity vectors for pin fin with spherical dimple configuration @ Re = 36700

The central high turbulence region was however distorted and elongated towards the dimple as seen in planes 1 – 3. This showed the dimples tried to pull the flow into the concavity. As the flow passed into the dimple, two counter rotating vortical structures were formed inside the concavity.

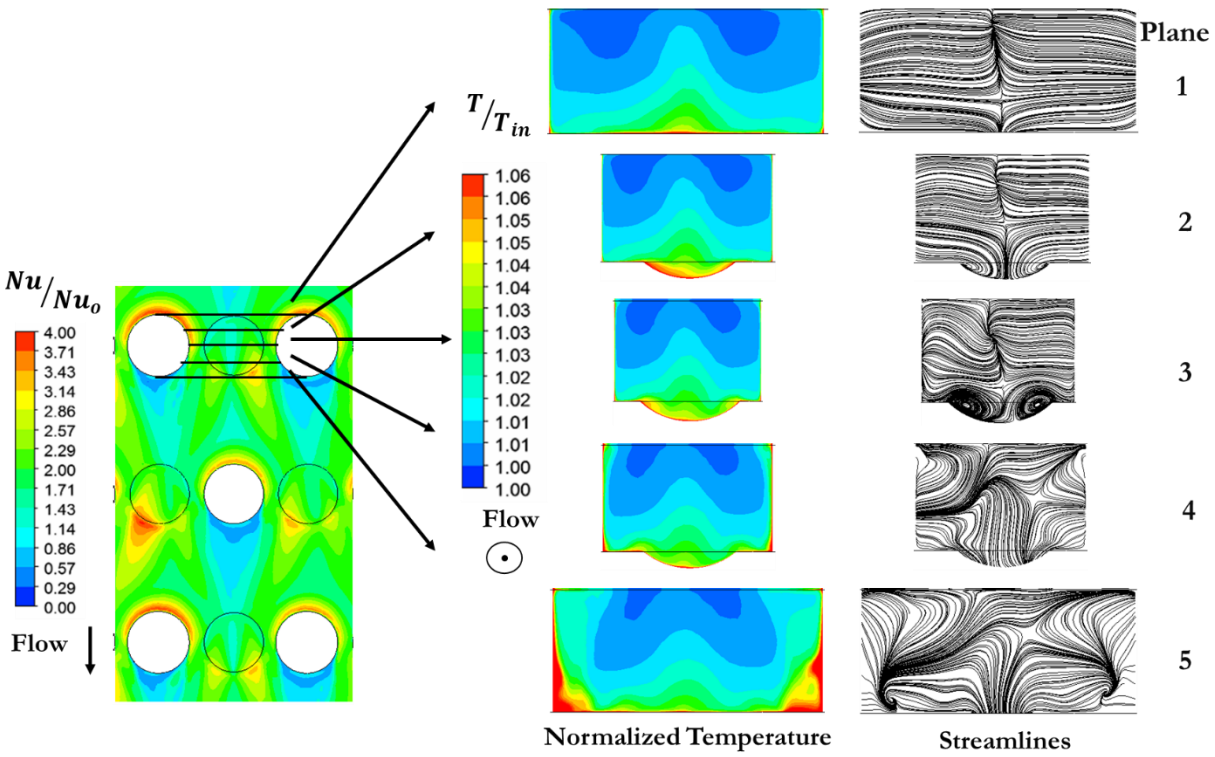

Figure [14]: Normalized Temperature and streamlines for pin fin with spherical dimple configuration @ Re = 36700

Regions of high turbulence were seen close to the dimple edges while due to the recirculation, the dimple walls experienced slower movement of the secondary flow. As the flow leaves the dimple cavity, it can be seen that the downstream edge of the dimple experienced high turbulence which extended up to 2/3 D_h inside the primary flow. These regions of high turbulence were mainly associated with large Nusselt number values as the flow provided a scrubbing effect to the primary flow and resulting in increased heat transfer in those regions.

Pin fin + cylindrical Dimple:

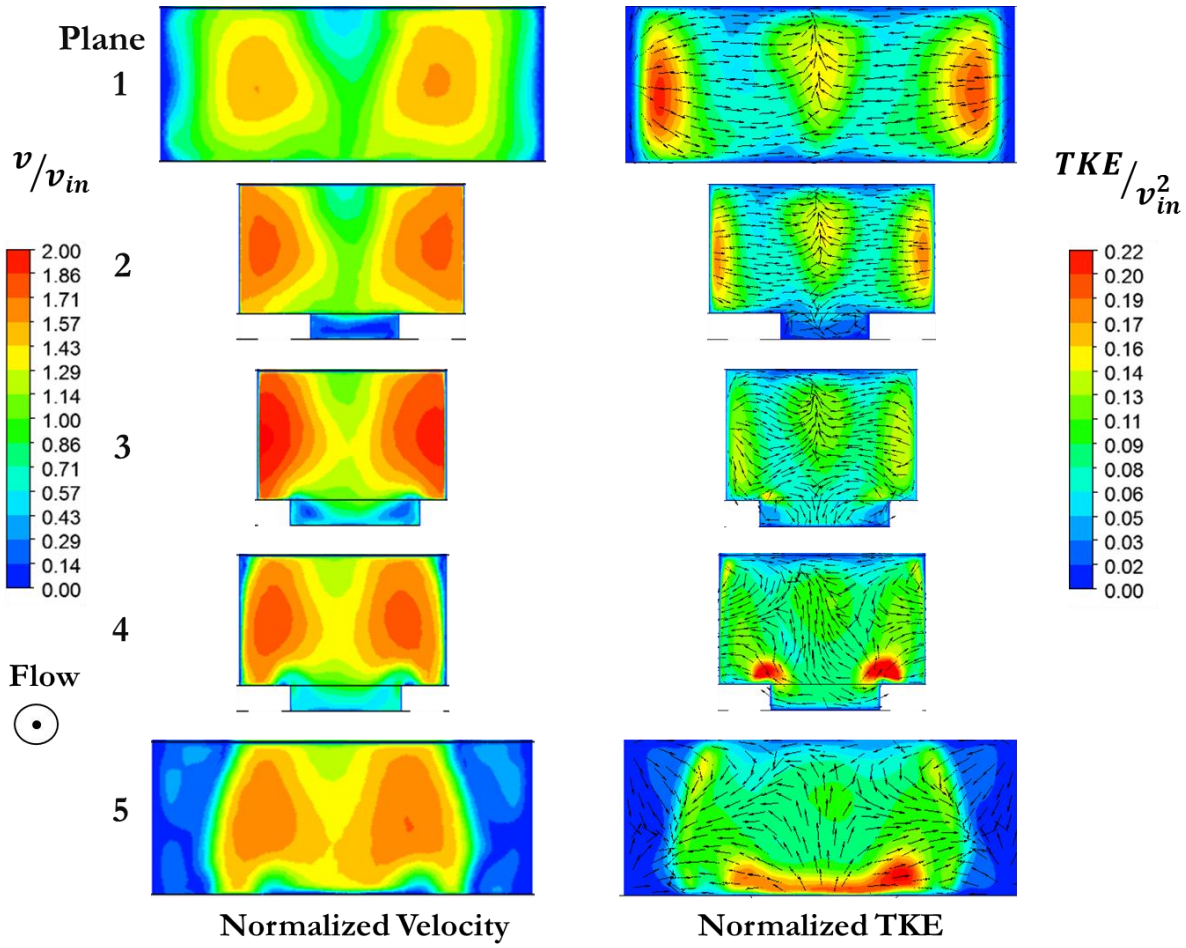

Figure [15]: Normalized velocity and turbulent kinetic energy superimposed with tangential velocity vectors for pin fin with cylindrical dimple configuration @ Re = 36700

Figure [14, 16, 18] representing temperature distribution show similar contours. Region of flow recirculation is seen inside the dimple which results in low heat dissipation rates and hence high temperatures. Enhanced bulk mixing due to the presence of dimple is seen in pin fin with dimple configurations which result in high temperature penetrating up to 2/3 rd of the channel height.

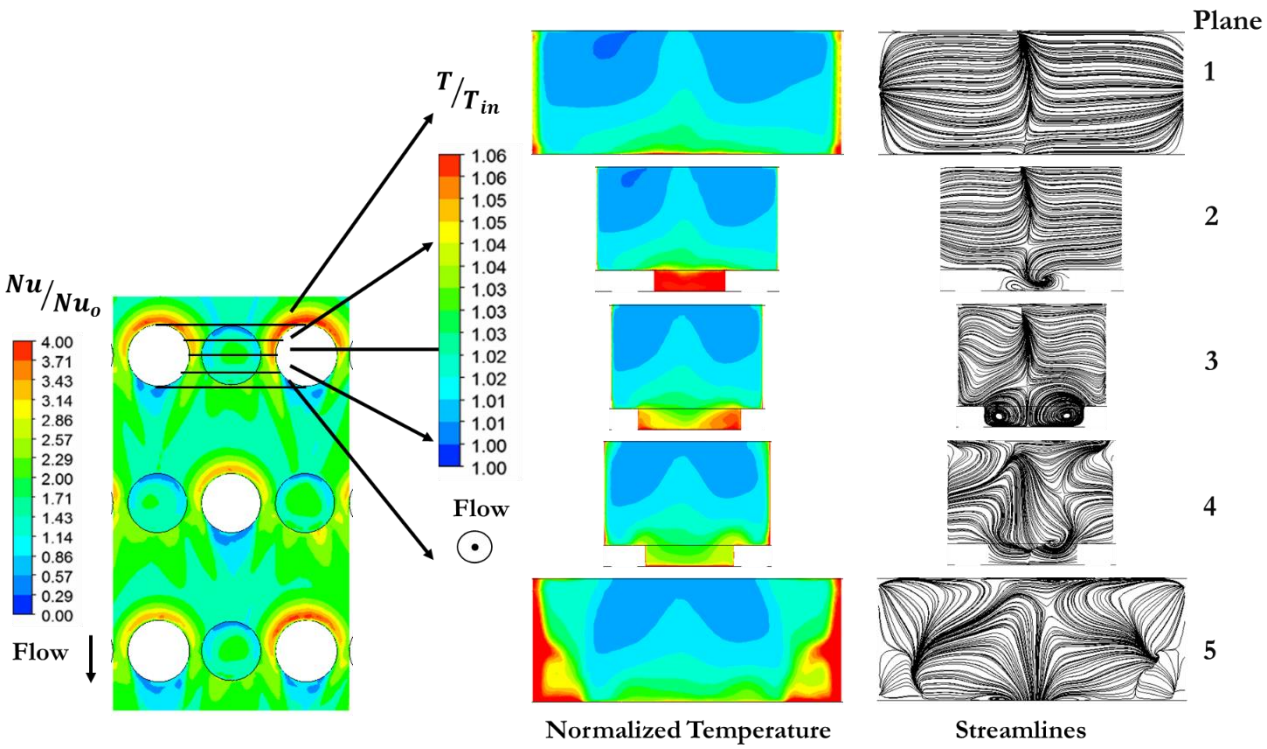

Figure [16]: Normalized Temperature and streamlines for pin fin with cylindrical dimple configuration @ Re = 36700

Division of the streams coming out of the dimple and joining the primary flow was apparent in all the three cases. From streamlines, it can be seen that a single vortex roll was found to be ejecting out of the spherical dimple while two vortex rolls coming out of the cylindrical and v-slot dimple were observed. The regions of high turbulence kinetic energy downstream of the dimples penetrate to a greater distance in the channel in case of pin fin with cylindrical dimple and that with v-slot dimple as compared to that in case of spherical dimple case.

Pin fin + v-slot Dimple:

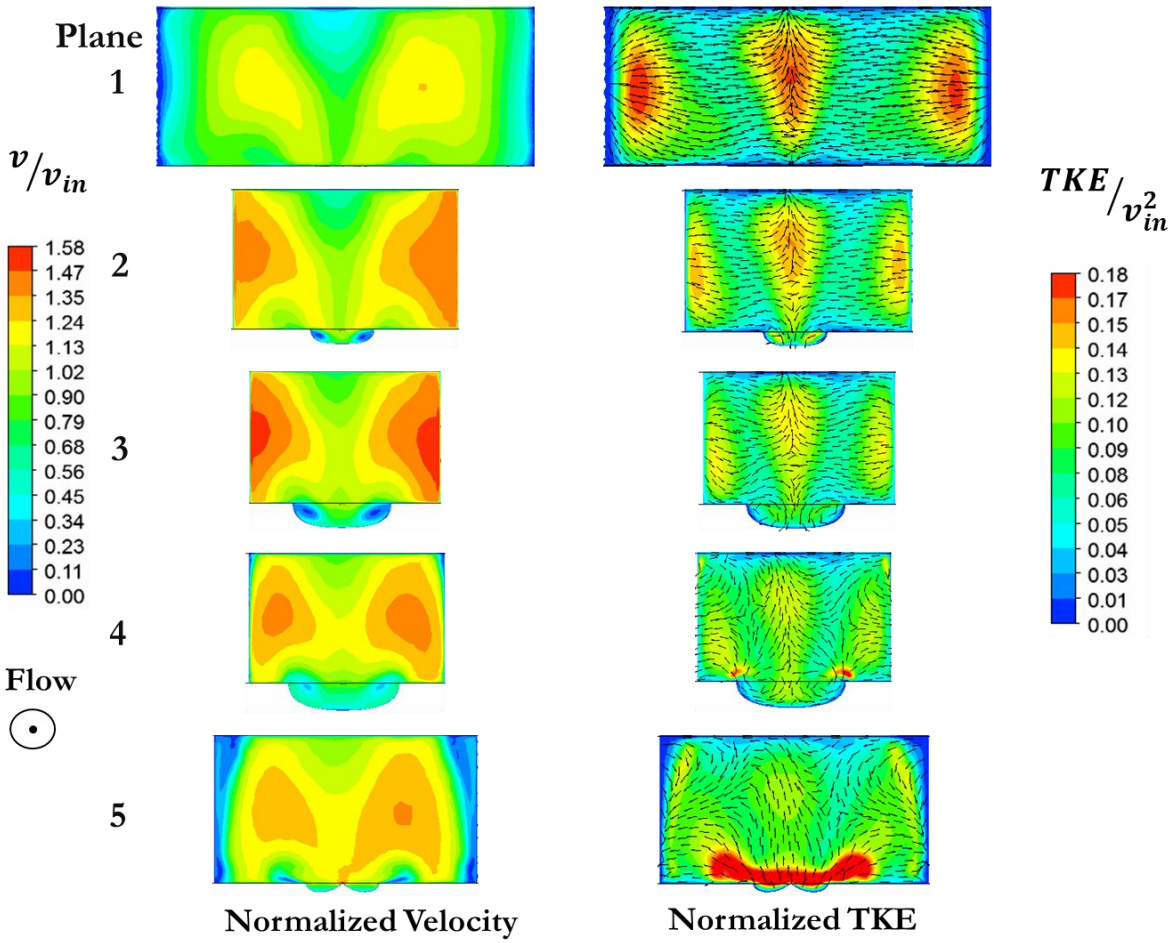

Figure [17]: Normalized velocity and turbulent kinetic energy superimposed with tangential velocity vectors for pin fin with v-slot dimple configuration @ Re = 36700

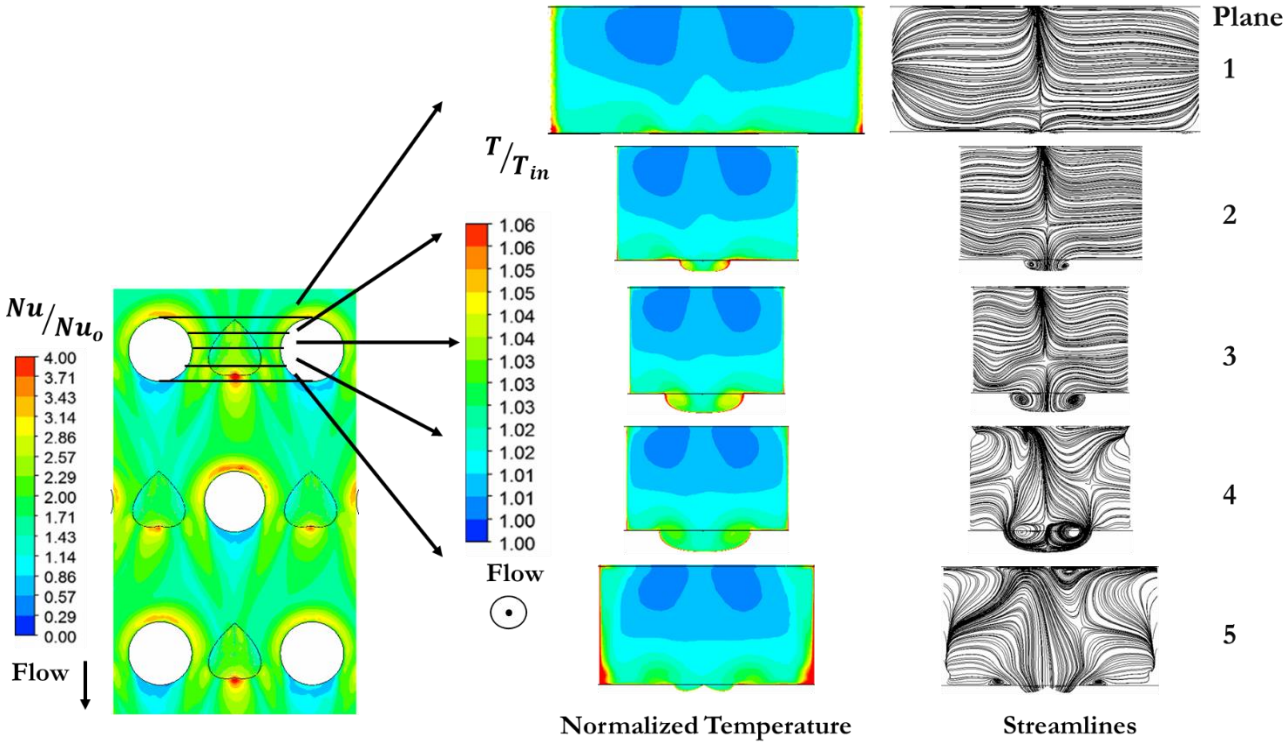

Figure [18]: Normalized Temperature and streamlines for pin fin with v-slot dimple configuration @ Re = 36700

In order to the study comparative the trends for the normalized velocity, temperature and turbulent kinetic energy for all configurations, contours have been plotted on a plane denoted in Fig. [7]. All the contours are taken at Reynolds number of Re = 36700. It can be seen that dimple has lowest levels of turbulence kinetic energy and velocity, while it has high temperature inside the dimple. From the temperature contour it is seen that inside v-slot dimples, only the side values have high temperature while the regions in the middle of the dimple wall have low values signifying high heat dissipation rates in those regions. This is not seen in other configurations of pin fin with spherical dimple and cylindrical dimple which show high temperatures along the wall as well as inside the dimple.

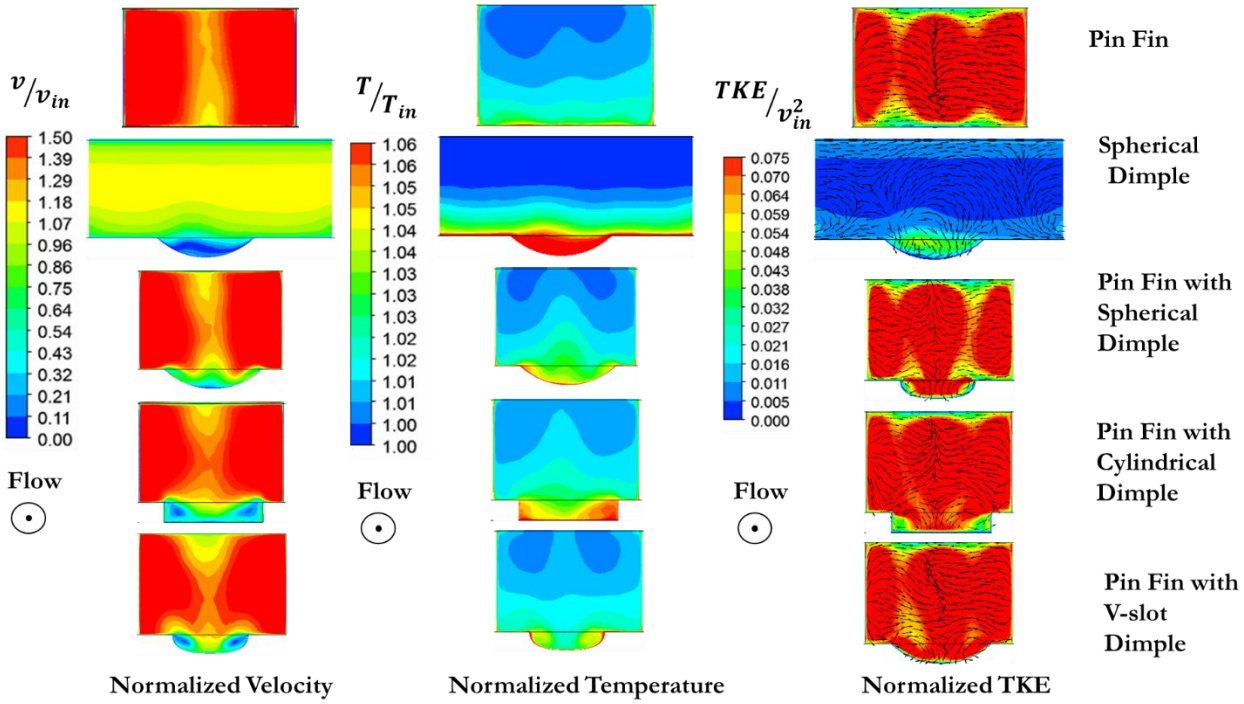

Figure [19]: Comparison of normalized velocity, temperature and turbulence kinetic energy for all configurations @ Re = 36700 on plane 3

Figure [20] show the plot of normalized temperature on plane P [1] as shown in Fig. [7]. This plot shows the high temperature regions inside the dimple concavities which correspond to recirculation regions. Regions of higher temperature upstream of the dimple were seen in case of pin fin with cylindrical dimple and only spherical dimple configurations. Also high temperature regions were witnessed in the wake region of the pin fins in the case of pin fin with dimple configurations. These recirculation regions resulted in lower Nusselt number values.

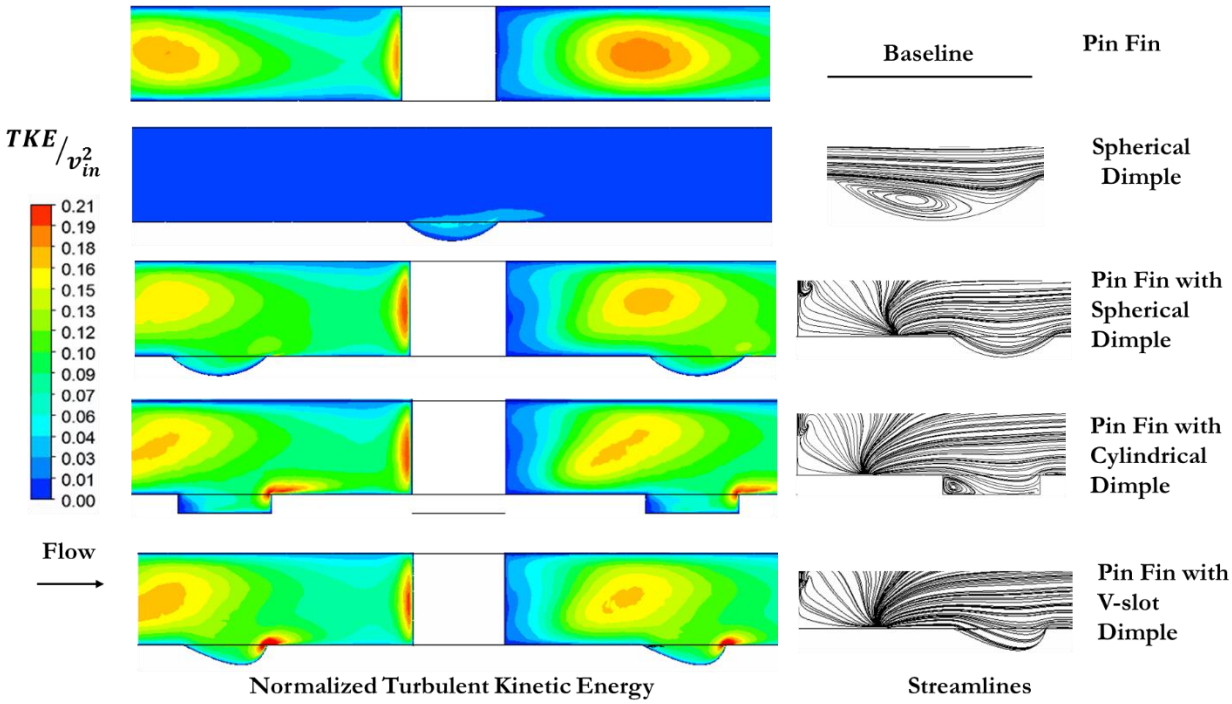

Figure [20]: Normalized turbulent kinetic energy and velocity superimposed with streamlines and tangential velocity vectors for all configurations at symmetry plane (streamwise) @ Re = 36700

Heat Transfer Enhancement: Nusselt Number

A correlation was developed in order to understand the scaling of Nu with Re,. Bunker et al. conducted a similar study to find out this scaling factor in various configurations in constant flow area channel which smooth plate and hemispherical concavity. The scaling factor was seen to be 0.81 for smooth plate close to that found in present study and 0.85 for hemispherical concavity. They also mentioned that the values of Nusselt number in their case were lower than those seen in Chyu et al's [5] research. However, they attributed this difference to the surface density and the d/D ratio in the two configurations.

It is important to mention that in Metzger et al's study, only bottom surface was considered for average Nusselt number calculations in order to develop the correlation. A similar practice has been adopted in current study to develop the correlation, also it should be noted that the correlation is based on only 4 points and there is a need to get more data points in order to come up a more reliable

correlation. Figure [21] shows a close match between the scaling factor seen in Metzger et al's study (0.728) and that obtained from simulations (0.7268) in this study. Also scaling factors in the range of 0.7 ~ 0.75 are seen for pin fin with dimple configurations which are comparable to those seen in pin fin and spherical dimple configurations.

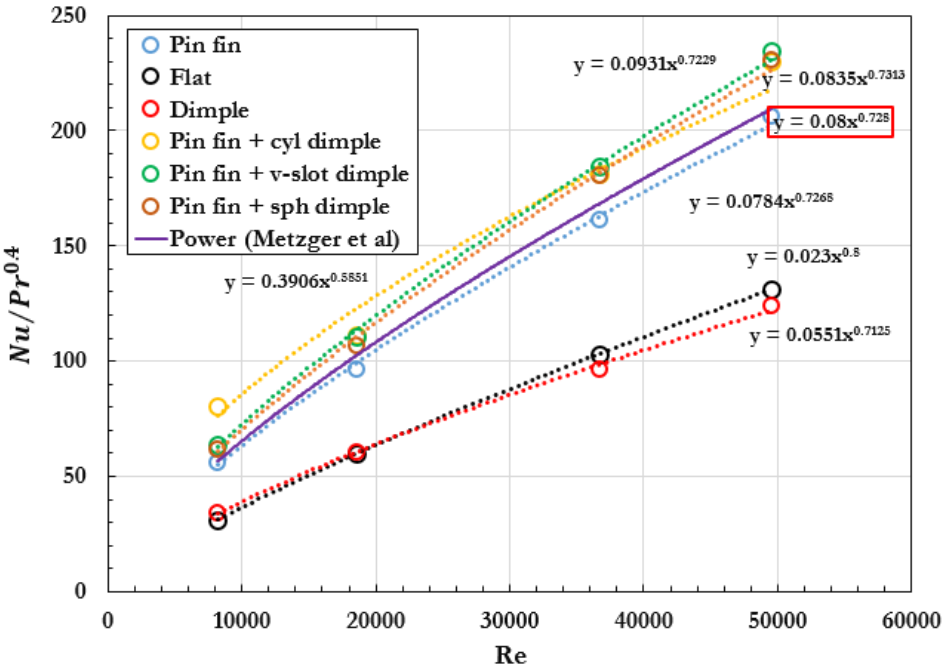

Figure [21]: Variation of average Nusselt number (calculated on bottom surface with considering enhancement due to features) with Re for all configurations

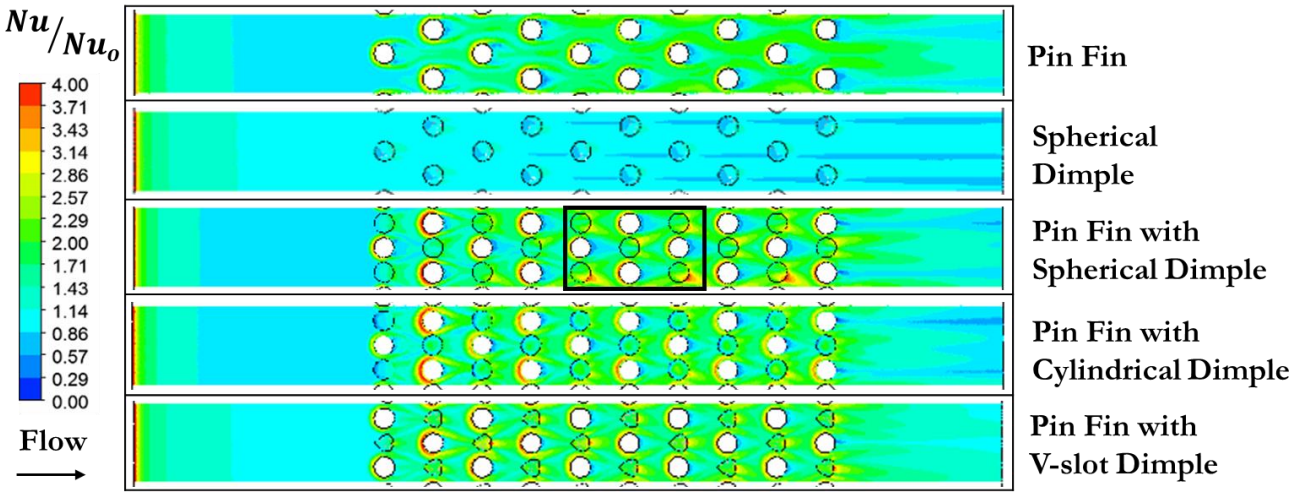

Figure [22]: Nusselt number enhancement (Periodicity in the flow) @ Re = 36700

Figure [22] shows the Nusselt number distribution for all configurations at Reynolds number of 36700. It can be seen from the contours that the Nusselt number distribution shows periodicity after 4th row. It has been mentioned before that the flow is thermally and hydraulically developing as it reaches first row which is a typical scenario in gas turbines trailing edge cooling. Also it has been seen that similar entrance condition prevail in several thermoelectric generator applications.

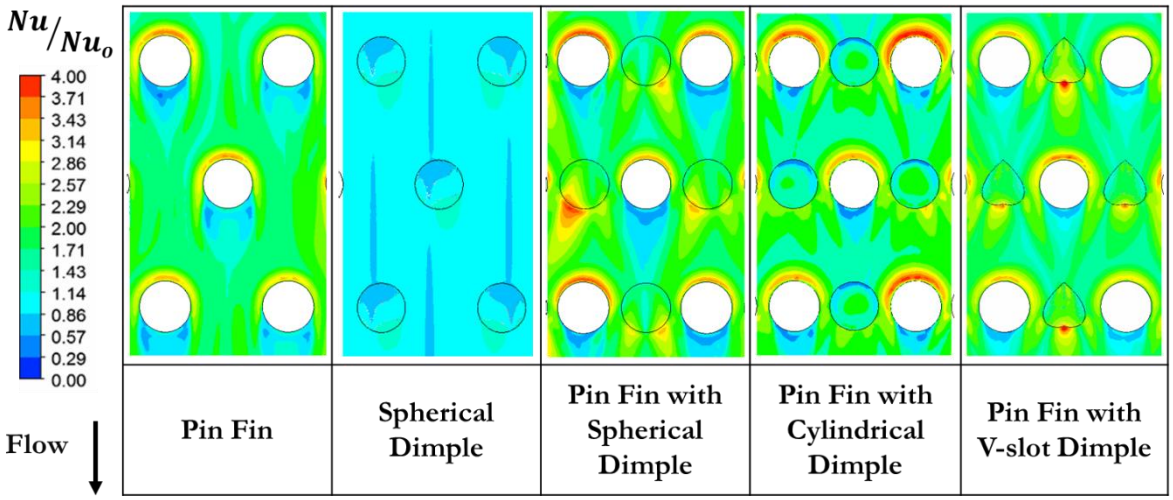

Figure [23]: Nusselt number contour for all configurations

In Fig. [23], Nu ratio is less than unity (between 0.5- 0.8) on the upstream half of the dimple bottom surface and is greater than unity (about 1.6) in most of the regions immediate downstream. High Nu ratio values were observed on the edge of the dimple. Similar characteristics were seen by Zhou et al, which is attributed to the slight flow impingement as the flow passages through the dimple. The upstream inside wall experiences Nu ratio lower than unity due to the flow separation occurring close to the upstream part of the dimple.

For pin fin case , high Nu ratio values were seen near the upstream half of the pin fin (stagnation region) and values lower than unity for Nu ratio are seen in the downstream half (wake region). It was seen in Figs. [6,7] that the presence of the dimples, affects the extent of the wake region. This turns out to be beneficial for uniform Nusselt number distribution, as the wake region is mainly associated with low Nusselt number values. As compared to pin fins, this region of reduced Nu extends over a shorter distance for pin fin dimple configuration. Thus making the surface distribution of Nusselt number more uniform. It can thus be said that pin fin dimple configurations, attempt at solving the

main objectives of current study by minimizing the area of low heat transfer coefficient and achieving uniform distribution of heat transfer coefficient. Though it should be noted that Nusselt number indicated in the figure above and frequently used for comparing configurations in this study is merely a measure of heat transfer coefficient and does not give any indication about the actual heat transfer rate.

High Nu values are seen at the edge of dimples in case of pin fin with dimple configurations. Low values of Nu ratio are seen on the upstream dimple edges. Thus it can be concluded that the effect of both pin fin and dimple are retained to certain extent in pin fin dimple configuration. For pin fin with dimple configurations, the wake length for pin fins is reduced and the extent of high Nu ratio region downstream of dimple is pronounced. While the Nu ratio in the upstream and downstream region of the dimple has increased in case of pin fin with dimple configurations, we can also see increased Nu ratio inside the dimple cavities. Average Nu enhancement in the range of the 2 – 2.5 is seen for Re = 36700 for pin fin with dimple configurations. Chyu et al has reported similar values for heat transfer coefficient enhancement in case of tear drop concavities.

Average Nusselt Number Variations

The surface averaged Nusselt number ratio is plotted in Fig. [24,25] as a function of Reynolds number. Figure [24] shows the ratio for nu averaged over the entire bottom wall including the features (sidewalls of pin fin and dimple cavity), while Fig. [25] represents ratio of nu averaged over the bottom surface without considering features. A decreasing trend with Reynolds number is seen for all configurations. A similar trend was seen for staggered array of v-slot dimples in case of Brown et al's [18] study. However, they reported lower heat transfer coefficient enhancement values for Re < 20000. It can be said that staggered arrays of dimples as relatively insensitive to the changes in Reynolds number as it is seen that the enhancement does not vary significantly for spherical dimple case. However, this is not the case with other configurations which show large deviations from insensitivity. From Fig. [24] it is seen that pin fin with v-slot dimples outperform other configurations if we consider the entire surface area of the bottom wall without excluding dimple cavities and pin fin side walls. Nusselt number enhancement for pin fin with v-slot dimple was 3% higher than pin fin with cylindrical dimple , 28% higher than pin fin with spherical dimple , 39 % higher than pin fin and 178% higher

than spherical dimple at Re = 8200. Dimples give considerably lower values which has been seen frequently in dimple studies in literature.

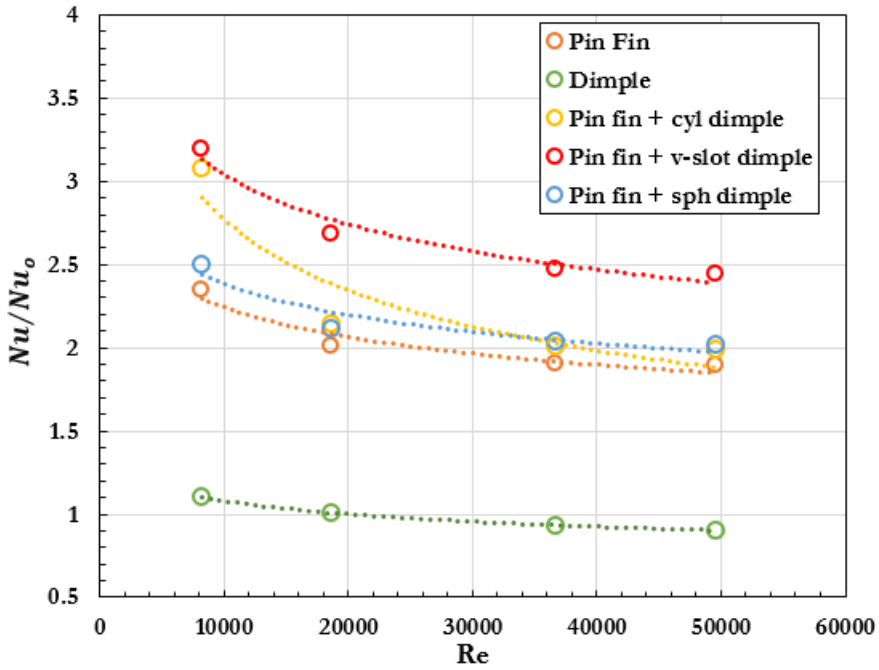

Figure [24]: Variation of Nusselt number enhancement ratio (calculated on the entire bottom surface including enhancement due to features) with Re for all configurations

Figure [25] , however shows that the pin fin with cylindrical dimple shows highest enhancement at low Reynolds number as compared to other configurations followed by pin fin with v-slot dimple and pin fin with spherical dimple showing almost similar values. It should be noticed that the rate at which the enhancement drops with Reynolds number is steep for pin fin with cylindrical dimple as compared to other configurations.

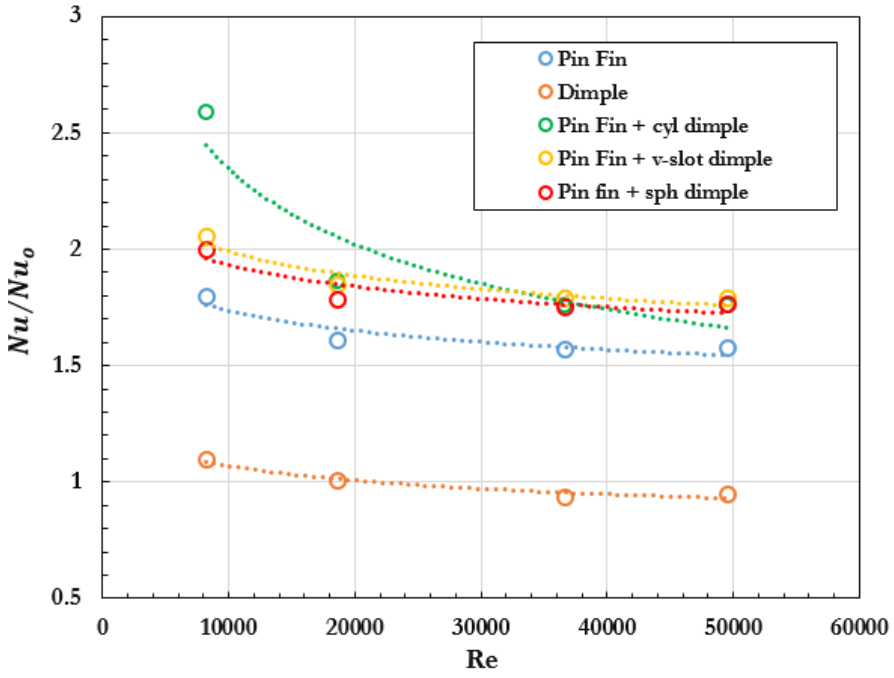

Figure [25]: Variation of Nusselt number enhancement ratio (calculated only on bottom surface without including enhancement due to features) with Re for all configurations

Pressure Loss

Figure [26] presents the friction factor values for all configurations. It can be commented that friction factor does not change a lot for dimple configuration. However, all the other configurations show a decreasing trend of friction factor with Reynolds number. Similar values were seen for friction factor for dimples by Bunker et al [38]. They saw values as high as 0.3 for friction factor in case of large diamond pin fins and compound feature arrays containing dimples and turbulators. In this study values way lower than 0.15 are seen which indicates low cost of Nusselt number enhancement. Highest pressure penalty was seen for pin fin with cylindrical dimple and pin fin with spherical dimple configuration which was 15 % higher than pin fin with v-slot dimple at Re = 8200.

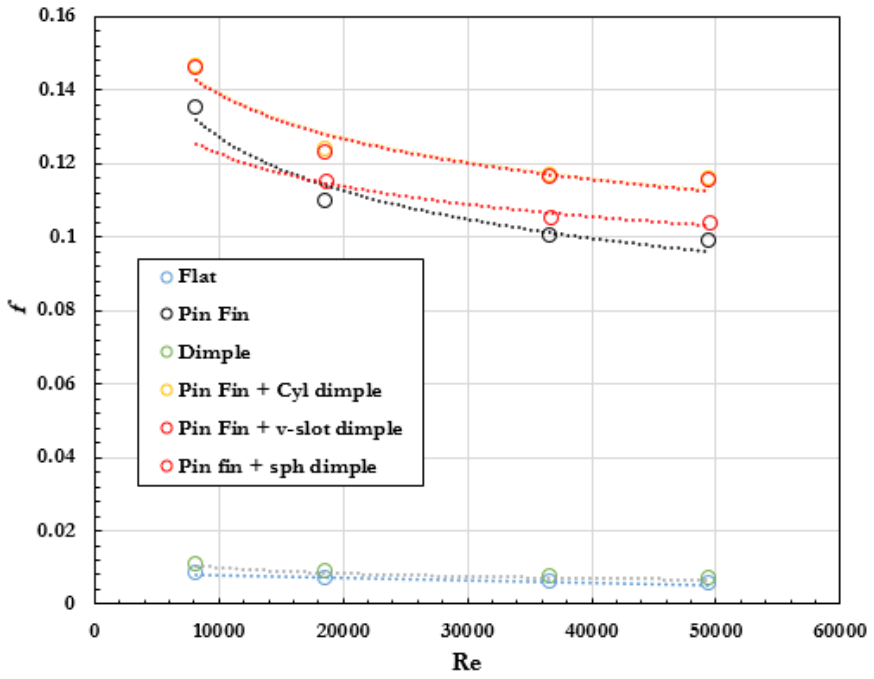

Figure [26]: Variation of friction factor with Re for all configurations

Overall Performance (Performance Factor Comparison)

Thermal performance of various configurations gives an indication of their thermal hydraulic performance by taking into consideration the Nusselt number enhancement as well as the friction factor. As against the trend seen for low values of Nusselt number enhancement in dimples, the thermal hydraulic performance shows higher values. This is one of the attractive features of dimples, to provide Nusselt number enhancement at low pressure penalties, which has made dimples popular among researchers. In Fig. [27,28] though overall performance values are lower as compared to that seen in literature Chyu et al ,concavity enhanced heat transfer] for tear shaped, hemispherical concavities and rib turbulators. Figure [27] shows that overall thermal-hydraulic performance was highest for pin fin with v-slot dimple and lowest for pin fin configuration. Literature shows that it is difficult to get Nusselt number information inside the dimples and hence most of the researchers generally use average Nusselt number over the bottom surface without taking into consideration enhancement due to the features to calculate overall performance. This can be misleading which is highlighted by Fig. [28], which shows overall performance calculated considering Nusselt number enhancement on the bottom surface (without features). Figure [28] shows that dimples out perform all other configurations which differs from the inference from Fig. [19].

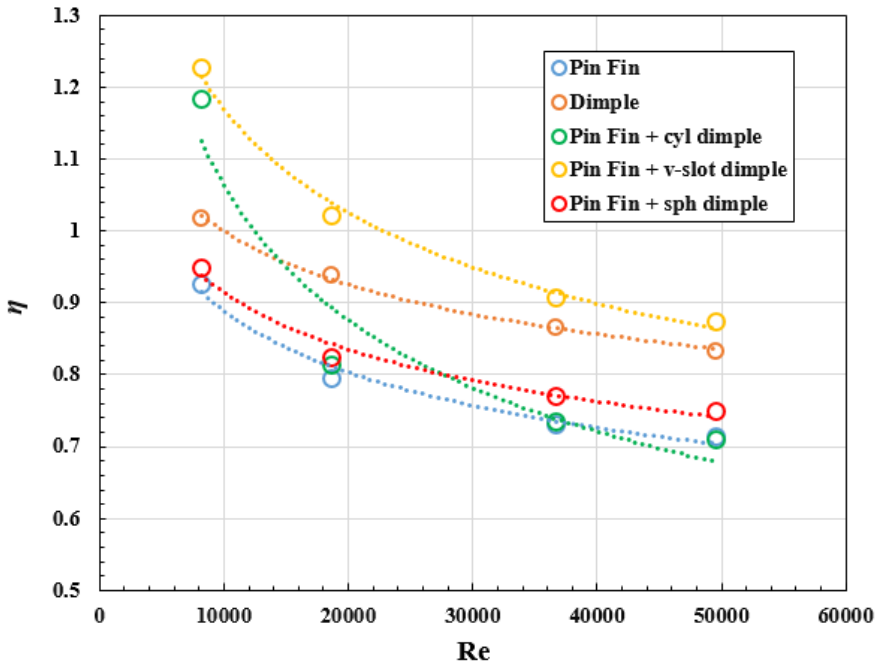

Figure [27]: Variation of thermal-hydraulic efficiency (calculated on entire bottom surface including enhancement due to features) with Re for all configurations

Features which protrude perpendicular into the flow domain like pin fins and rib turbulators are associated with high levels of turbulence along with increase in the wetted surface area normal to the flow. This results in increased Nusselt number enhancement values however, they also cause large amounts of pressure drop. On the other hand concavities provide low Nusselt number enhancement but with much lesser pressure drop as compared to other Nusselt number enhancement features. This enhancement can be attributed to the increase in area and the results not so strong secondary flows. These results have been reported by Bunker et al.

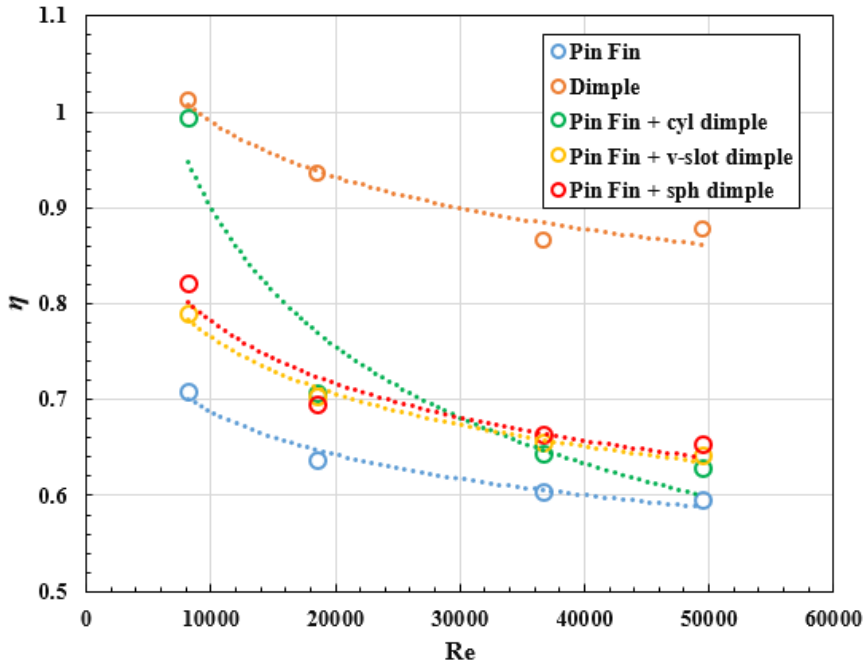

Figure [28]: Variation of thermal-hydraulic efficiency (calculated only on bottom surface without including enhancement due to features) with Re for all configurations

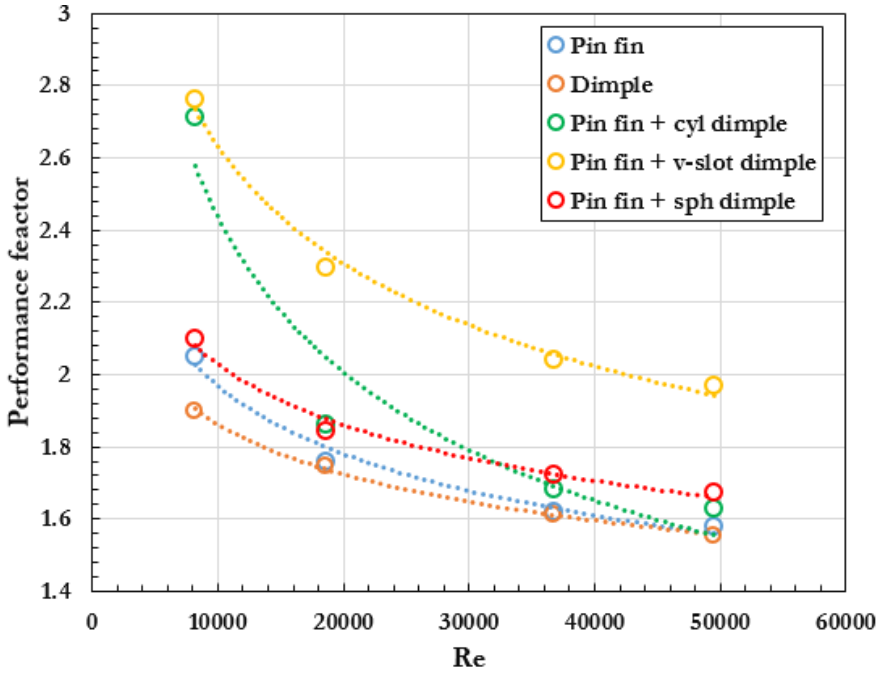

Figure [29]: Variation of performance factor (calculated on entire bottom surface including enhancement due to features) with Re for all configurations

It can be seen in Table [2] that the ratio of the wetted area varies in case of various configurations. The location and the side wall area of pin fins has been kept constant in all the configurations and only the shape of dimples has been varied. In order to understand the combined effect of heat transfer, surface area and low friction factor, Bunker et al came up with a factor called as performance factor which is given by equation (6). An increasing trend was seen in case of pin fins while the combination of pins and dimples as well as dimpulators showed a decreasing trend with Reynolds number in his study. In Fig. [29] , a decreasing trend for performance factor with Reynolds number is seen, this difference in the trend can be attributed to various factors like height of the pin fin, surface density. Pin fin with v-slot dimple shows higher values than all the other configurations. Pin fin with cylindrical dimple performance is second best followed by pin fin with spherical dimple and lowest values for dimple configuration.

CONCLUSIONS

Flow field and heat characteristics for compound modes of enhancement have been investigated in this study. Four configurations viz. pin fin, spherical dimple, pin fin with spherical dimple, pin fin with cylindrical and pin fin with v-slot dimple have been analyzed over a wide range of Reynolds number from 8200 to 49500. Flow was thermally and hydraulically developing as it approached the first row of features. Good agreement was observed between the simulations and literature where the model was able to predict the flow and nusselt number distribution. The interaction of the dimple and pin fin induced secondary flow was studied for configurations. In conventional pin fin configurations, it was seen that wake region extended beyond half the stream wise pitch. It was seen that the flow and the heat transfer in the combined mode of heat enhancement (pin fin with dimple configurations) were similar. Similarly spherical dimple have low levels of heat transfer enhancement inside the dimples, however these levels improved in case of combined mode of enhancements. Detailed flow field and heat transfer characteristics have been presented in this study, which would be useful in optimization of combined mode of enhancement. It was seen that Nusselt number enhancement reduced with Reynolds number. Highest Nusselt number enhancement was seen for pin fin with v-slot dimple which was 3% higher than pin fin with cylindrical dimple , 28% higher than pin fin with spherical dimple , 39 % higher than pin fin and 178% higher than spherical dimple at Re = 8200. Highest pressure penalty was seen for pin fin with cylindrical dimple and pin fin with spherical dimple configuration which was 15 % higher than pin fin with v-slot dimple at Re = 8200. Overall thermal-

hydraulic performance was highest for pin fin with v-slot dimple and lowest for pin fin configuration. On comparing the performance factor based on the area enhancement due to the features, Pin fin with v-slot dimple performed better than other configurations.

REFERENCES

[1] Arik, M., and Bunker, R., 2006, "Electronics Packaging Cooling: Technologies from Gas Turbine Engine Cooling", Journal of electronic packaging 128(3), pp. 215-225.

[2] Schukin, A. V., Kozlov A. P., and Agachev R. S., 1995, "Study and Application of Hemispheric Cavities for Surface Heat Transfer Augmentation", ASME 1995 International Gas Turbine and Aeroengine Congress and Exposition. American Society of Mechanical Engineers.

[3] Terekhov, Viktor I., Kalinina. S. V., and Mshvidobadze. Yu M., 1997, "Heat Transfer Coefficient and Aerodynamic Resistance on a Surface with a Single Dimple", Journal of Enhanced Heat Transfer., 4(2).

[4] Nagoga, G. P., 1996, "Effective Methods Of Cooling Of Blades Of High Temperature Gas Turbines", Publishing House of Moscow Aerospace Institute (Russian language), 100.

[5] Chyu, M. K., Yu, Y., Ding, H., Downs, J. P.,Soechting, F. O. 1997, "Concavity Enhanced Heat Transfer In An Internal Cooling Passage." ASME 1997 International Gas Turbine and Aeroengine Congress and Exhibition. American Society of Mechanical Engineers.

[6] Zhou, Fuguo, and Acharya. S., 2009, "Experimental and Computational Study of Heat/Mass Transfer and Flow Structure for Four Dimple Shapes in a Square Internal Passage." ASME Turbo Expo 2009: Power for Land, Sea, and Air. American Society of Mechanical Engineers.

[7] Moon, H. K., O'Connell T., and Glezer. B., 2000, "Channel Height Effect On Heat Transfer And Friction In A Dimpled Passage", Journal of Engineering for Gas Turbines and Power 122(2), pp. 307-313.

[8] Lin, Y-L., Shih, T. IP., and Chyu M. K., 1999, "Computations Of Flow And Heat Transfer In A Channel With Rows Of Hemispherical Cavities." ASME 1999 International Gas Turbine and Aeroengine Congress and Exhibition. American Society of Mechanical Engineers.

[9] Mahmood, G. I., et al., 2000, "Local Heat Transfer And Flow Structure On And Above A Dimpled Surface In A Channel." ASME Turbo Expo 2000: Power for Land, Sea, and Air. American Society of Mechanical Engineers.

[10] Choudhury, D., and Karki. K. C., 1991, "Calculation Of Fully Developed Flow And Heat Transfer In Streamwise-Periodic Dimpled Channels." Journal of thermophysics and heat transfer, 5(1), pp. 81-88.

[11] Ligrani, P. M., 2001, "Flow Structure Due To Dimple Depressions On A Channel Surface." Physics of Fluids (1994-present), 13(11), pp. 3442-3451.

[12] Isaev, S. A., Leont'ev. A. I., and Baranov. P. A., 2000, "Identification Of Self-Organized Vortex Like Structures In Numerically Simulated Turbulent Flow Of A Viscous Incompressible Liquid Streaming Around A Well On A Plane." Technical physics letters 26(1), pp. 15-18.

[13] Syred, N., et al., 2000, "Effect Of Surface Curvature On Heat Transfer And Hydrodynamics Within A Single Hemispherical Dimple." ASME Turbo Expo 2000: Power for Land, Sea, and Air. American Society of Mechanical Engineers.

[14] Zhou, Fuguo, and Acharya. S., 2001, "Mass/Heat Transfer In Dimpled Two-Pass Coolant Passages With Rotation." Annals of the New York Academy of Sciences, 934(1). pp. 424-431.

[15] Isaev, Aleksandrovich. S., and Leont'ev. A. I., 2003, "Numerical Simulation Of Vortex Enhancement Of Heat Transfer Under Conditions Of Turbulent Flow Past A Spherical Dimple On The Wall Of A Narrow Channel." High Temperature 41(5), pp. 665-679.

[16] Bunker, Ronald S., et al., 2003, "Heat Transfer And Pressure Loss For Flows Inside Converging And Diverging Channels With Surface Concavity Shape Effects", Proceedings of the 4th International Conference on Compact Heat Exchangers and Enhancement Technology, Crete Island, Greece.

[17] Case, L, Jordan C. N., and Wright. L., 2011, "Effect of Dimple Depth on Heat Transfer Enhancement in A Rectangular Channel (Ar= 3: 1) With Hemispherical Dimples", 49th AIAA Aerospace Sciences Meeting including the New Horizons Forum and Aerospace Exposition.

[18] Brown, Charles P., Wright, L M., and McClain. S T., 2015, "Comparison Of Staggered And In-Line V-Shaped Dimple Arrays Using S-PIV." ASME Turbo Expo 2015: Turbine Technical Conference and Exposition. American Society of Mechanical Engineers.

[19] Jordan, Neil C., and Wright, L M., 2013, "Heat Transfer Enhancement In A Rectangular (AR= 3: 1) Channel With V-Shaped Dimples." Journal of Turbomachinery 135(1). pp. 011028.

[20] Žukauskas, A., 1972, "Heat Transfer From Tubes In Crossflow." Advances in heat transfer 8, pp. 93-160.

[21] Lau, S. C., Kim, Y. S., and Han, J. C., 1987, "Local Endwall Heat/Mass Transfer In A Pin Fin Channel.", Heat transfer and fluid flow in rotating machinery, 1, pp. 64-75.

[22] VanFossen, G. J., 1982, "Heat-Transfer Coefficients For Staggered Arrays Of Short Pin Fins", Journal of Engineering for Power, 104(2), pp. 268-274.
[23] Brigham, B. A., and VanFossen, G. J., 1984, "Length To Diameter Ratio And Row Number Effects In Short Pin Fin Heat Transfer", Journal of Engineering for Gas Turbines and Power, 106(1), pp. 241-244.
[24] Simoneau, R. J., and Vanfossen Jr, G. J., 1982, "Effect Of Location In An Array On Heat Transfer To A Cylinder In Crossflow"
[25] Sparrow, E. M., and Ramsey, J. W., 1978, "Heat Transfer And Pressure Drop For A Staggered Wall-Attached Array Of Cylinders With Tip Clearance", International journal of heat and mass transfer, 21(11), pp. 1369-1378.
[26] Sparrow, E. M., Ramsey, J. W., and Altemani, C. A. C., 1980, "Experiments On In-Line Pin Fin Arrays And Performance Comparisons With Staggered Arrays", Journal of Heat Transfer, 102(1), pp. 44-50.
[27] Metzger, D. E., Berry, R. A., and Bronson, J. P., 1982, "Developing Heat Transfer In Rectangular Ducts With Staggered Arrays Of Short Pin Fins.", Journal of Heat Transfer, 104(4), pp. 700-706.
[28] Metzger, D. E., Fan, Z. X., and Shepard, W. B., 1982, "Pressure Loss And Heat Transfer Through Multiple Rows Of Short Pin Fins", Heat Transfer 1982, 3, pp. 137-142.
[29] Chyu, M. K., Hsing, Y. C., Shih, T. P., and Natarajan, V., 1999, "Heat Transfer Contributions Of Pins And Endwall In Pin-Fin Arrays: Effects Of Thermal Boundary Condition Modeling", Journal of Turbomachinery, 121(2), pp. 257-263.
[30] Lawson, S. A., Thrift, A. A., Thole, K. A., and Kohli, A., 2011, "Heat Transfer From Multiple Row Arrays Of Low Aspect Ratio Pin Fins.", International Journal of Heat and Mass Transfer, 54(17), pp. 4099-4109.
[31] Ostanek, J. K., and Thole, K. A., 2012, June, "Effects Of Varying Streamwise And Spanwise Spacing In Pin-Fin Arrays.", ASME Turbo Expo 2012: Turbine Technical Conference and Exposition. American Society of Mechanical Engineers. , pp. 45-57.
[32] Lyall, M. E., Thrift, A. A., Thole, K. A., and Kohli, A., 2011, "Heat Transfer From Low Aspect Ratio Pin Fins", Journal of Turbomachinery, 133(1), pp. 011001.
[33] Metzger, D. E., Fan, C. S., and Haley, S. W., 1984, "Effects Of Pin Shape And Array Orientation On Heat Transfer And Pressure Loss In Pin Fin Arrays", Journal of Engineering for Gas Turbines and Power, 106(1), pp. 252-257.

[34] Chyu, M. K., Hsing, Y. C., and Natarajan, V., 1996, "Convective Heat Transfer Of Cubic Fin Arrays In A Narrow Channel", ASME 1996 International Gas Turbine and Aeroengine Congress and Exhibition. American Society of Mechanical Engineers. , pp. V004T09A020-V004T09A020

[35] Kirsch, K. L., Ostanek, J. K., and Thole, K. A., 2014, "Comparison Of Pin Surface Heat Transfer In Arrays Of Oblong And Cylindrical Pin Fins", Journal of Turbomachinery, 136(4), pp. 041015.

[36] Taslim, M. E., Li, T., and Kercher, D. M., 1994, "Experimental Heat Transfer And Friction In Channels Roughened With Angled, V-Shaped And Discrete Ribs On Two Opposite Walls", ASME 1994 International Gas Turbine and Aeroengine Congress and Exposition. American Society of Mechanical Engineers, pp. V004T09A018-V004T09A018

[37] Mahmood, G. I., Sabbagh, M. Z., and Ligrani, P. M., 2001, "Heat Transfer In A Channel With Dimples And Protrusions On Opposite Walls", Journal of Thermophysics and Heat Transfer, 15(3), pp. 275-283.

[38] Bunker, R. S., Bailey, J. C., Lee, C. P., & Stevens, C. W. ,2004, "In-Wall Network (Mesh) Cooling Augmentation of Gas Turbine Airfoils", ASME Turbo Expo 2004: Power for Land, Sea, and Air, pp. 1007-1018

[39] Rao, Y., Wan, C., and Zang, S., 2010, "Comparisons Of Flow Friction And Heat Transfer Performance In Rectangular Channels With Pin Fin-Dimple, Pin Fin And Dimple Arrays", ASME Turbo Expo 2010: Power for Land, Sea, and Air. American Society of Mechanical Engineers, pp. 185-195.

[40] Rao, Y., Wan, C., Xu, Y., and Zang, S., 2011, "Spatially-Resolved Heat Transfer Characteristics In Channels With Pin Fin And Pin Fin-Dimple Arrays", International Journal of Thermal Sciences, 50(11), pp. 2277-2289.

[41] Rao, Y., Wan, C., and Xu, Y., 2012, "An Experimental Study Of Pressure Loss And Heat Transfer In The Pin Fin-Dimple Channels With Various Dimple Depths", International Journal of Heat and Mass Transfer, 55(23), pp. 6723-6733.

[42] Rao, Y., Wan, C., Xu, Y., and Zang, S., 2011, "Local Heat Transfer Characteristics In Channels With Pin Fin And Pin Fin-Dimple Arrays", ASME 2011 Turbo Expo: Turbine Technical Conference and Exposition. American Society of Mechanical Engineers. pp. 1205-1216

[43] Park, J., Desam, P. R., and Ligrani, P. M., 2004, "Numerical Predictions Of Flow Structure Above A Dimpled Surface In A Channel", Numerical Heat Transfer, Part A: Applications, 45(1), pp. 1-20.

[44] Xie, G., Sundén, B., and Zhang, W., 2011, "Comparisons Of Pins/Dimples/Protrusions Cooling Concepts For A Turbine Blade Tip-Wall At High Reynolds Numbers", Journal of Heat Transfer, 133(6), pp. 061902.

[45] Hansen, L. G., and Webb, B. W., 1993, "Air Jet Impingement Heat Transfer from Modified Surfaces", International journal of heat and mass transfer, 36(4), pp. 989-997.

[46] Metzger, D. E., and Haley, S. W., 1982, "Heat Transfer Experiments and Flow Visualization for Arrays of Short Pin Fins", ASME 1982 International Gas Turbine Conference and Exhibit. American Society of Mechanical Engineers, pp. V004T09A007-V004T09A007.

CHAPTER 2

EFFECT OF LONGITUDINAL VORTEX GENERATOR LOCATION ON THERMOELECTRIC- HYDRAULIC PERFORMANCE OF A SINGLESTAGE INTEGRATED THERMOELECTRIC POWER GENERATOR

Samruddhi Deshpande, Bharath Viswanath Ravi, Jaideep Pandit ,
Scott Huxtable, Srinath V. Ekkad

Department of Mechanical Engineering
Virginia Polytechnic Institute and State University
Blacksburg, Virginia, USA

Ting Ma

Department of Mechanical Engineering
Xi'an Jiaotong University,
Xi'an, Shaanxi 710049

ASME Paper No. IMECE2015-52244

ABSTRACT

Vortex generators have been widely used to enhance heat transfer in various heat exchangers. Out of the two types of vortex generators: Transverse vortex generators (TVGs) and longitudinal vortex generators (LVGs), LVGs have been found to show better heat transfer performance. Past studies have shown that the implementation of these LVGs can be used to improve heat transfer in thermoelectric generator systems. Here a built in module in COMSOL Multiphysics® was used to study the influence of the location of LVGs in the channel on the comprehensive performance of an integrated thermoelectric device (ITED). The physical model under consideration consists of a copper interconnector sandwiched between p-type and n- type semiconductors and a flow channel for hot fluid in the center of the interconnector. Four pairs of, LVGs are mounted symmetrically on the top and bottom surfaces of the flow channel. Thus, using numerical methods, the thermo-electric-hydraulic performance of the ITED with a single module is examined By fixing the material size D, the fluid inlet temperature T_{in}, and attack angle β; the effects of the location of LVGs and Reynolds number were investigated The location of LVGs did not have significant effect on the performance of TEGs in the given model. However, the performance parameters show a considerable change with Reynold's number and best performance is obtained at Reynold number of Re = 500.

NOMENCLATURE

c_p	= Specific heat, J/(kg·K)
D	= Thickness, mm
D_h	= Hydraulic diameter, mm
E	= Electric field intensity, V/m
H	= Height, mm
I	= Electric current, A
J	= Electric current density, A/m^2
K	= Thermal conductivity, W/(m·K)
L	= Length, mm
P	= Static pressure, Pa
P_l	= Longitudinal pitch, mm
P_o	= Power output, W
P_t	= Transverse pitch, mm
Q_h	= Hot-side heat transfer rate, W
Re	= Reynolds number
T	= Temperature, K
U	= Area-averaged velocity in inlet section, m/s
u	= Velocity vector, m/s
V	= Voltage, V
$\dot{V}$	= Volumetric flow rate, m^3/s
W	= Width, mm
W_{net}	= Net power, W
$W_{\Delta p}$	= Pumping power, W
Greek	
α	= Seebeck coefficient, V/K
β	= Attack angle, °
ρ	= Density, kg/m^3
σ	= Electrical conductivity, S/m
$\prod$	= Peltier coefficient, V
μ	= Dynamic viscosity, Pa·s
η	= Thermal conversion efficiency

Subscripts

c = Cold

f = Fluid

h = Hot

v = Longitudinal vortex generator

i = Interconnector

INTRODUCTION

In all combustion processes, a significant fraction of the initial chemical energy is lost as waste heat. Thermoelectric power generators have the ability to directly convert heat into electrical energy. Thus, thermoelectric generators (TEGs) can be employed to capture some of this otherwise wasted heat and to convert this heat into useful electrical energy. For example, TEGs have wide spread applications ranging from biomass cook stoves, to automobiles, to nuclear reactors. [1, 2, 3, 4, 5]. The performance of thermoelectric material can be quantified with a dimensionless figure of merit, ZT, which is defined as $ZT = \frac{\alpha^2 \sigma T}{\lambda}$ where α is the Seebeck coefficient, σ is the electrical conductivity, and λ is the total thermal conductivity. The numerator $\alpha^2\sigma$ is called the electrical power factor. The thermal efficiency of a thermoelectric generator is defined as the electrical power output divided by the heat input to the TEG. The thermal efficiency, η, of the TEG can also be approximated as [6]

$$\eta = \frac{\Delta T}{T_h} \frac{\sqrt{1+ZT}-1}{\sqrt{1+ZT}+\frac{T_c}{T_h}} \qquad (1)$$

where ΔT is the temperature gradient across the device, and T_c and T_h are the cold and hot side temperatures, respectively.

Hsiao et al. [7] developed a mathematical model of thermoelectric module, and their results showed the applicability of TEGs to extract energy from automobile exhaust. Wang et al. [8] presented a three dimensional numerical model of a thermoelectric device with consideration of coupling of the temperature field and the electric potential field. This model considered Joule heating, the Thomson effect, Fourier's heat conduction, the Peltier effect, radiation and convection heat transfer, and temperature dependent material properties. Thus, this model provided a realistic approach to the feasibility of TEG's for exhaust energy recovery. Chen et al. [9] developed a three-dimensional thermoelectric generator model and implemented it in ANSYS (FLUENT). Similar to the above models, this model accounts for temperature dependent characteristics of the materials, but it also

includes non-linear fluid-thermal-electric multi-physics coupled effects. User defined scalars were used to determine electric field produced by the Seebeck potential and electric current throughout the thermoelectric elements. Reddy et al. [10] studied the performance of Π shaped conventional and composite thermoelectric devices (TEDs). They showed that when the TE leg length is greater than optimum length, and the TED is operating under higher convective heat transfer conditions, the composite design exhibits better power output and lower conversion efficiency compared to the conventional design. The integrated TED is a composite TED with the interconnector designed as an internal heat exchanger with the flow channel directing the working fluid between the source and the element legs. An improved performance compared to conventional TEDs was noticed by Reddy et al. from this model [11, 12].

Pandit et al. [13] showed that an effective way to increase total power output was by enhancing heat transfer on the hot side of the TEG through a pin fin model. Mitra et al. [14] investigated the effect of longitudinal vortices generated by a rectangular winglet in transition channel flow on the flow structure, heat transfer, and drag. The heat transfer enhancement was seen to be 80 % and drag increased by 160 %, thus showing the feasibility of these features to be integrated in thermoelectric module. The heat transfer also showed enhancement with increasing Reynolds number. Numerical studies were carried out by Wu et al. [15] to see the effect of various parameters of winglet geometry on heat transfer enhancement and flow resistance in a rectangular channel. They found out that for a flow in a long channel, the heat transfer enhancement decreased as the distance of LVGs from the channel inlet increased.

Ma et al. [16] carried numerical simulations of a thermoelectric module taking into account the Seebeck, Peltier, and Thomson effects along with temperature dependent material properties. They integrated two pairs of LVGs in this thermoelectric module to enhance the heat transfer and the power output. Specifically, they studied the effect of the height of the LVGs, the Reynolds number, and the angle of attack on the performance. Their study showed that TEG with LVGs which span full height of flow channel and temperature at which it was examined set to 550 K gave best performance. Also they showed that the effect of LVG angle on the heat input and power output is minimal.

In this paper, the effect of the location of LVGs from inner flow channel inlet and the effect of longitudinal pitch on the heat transfer enhancement, power output, and pressure drop is investigated

.

Physical Model and Boundary Conditions

The baseline design of an integrated device without LVGs was proposed by Reddy et al. [10]. This design was then modified by Ma et al. [16] to include LVGs. Here the design proposed by Ma et al. [16], which is shown in Figure 1, is used. In this model, a copper interconnector is sandwiched between p-type and n-type semiconductors and a hot fluid is passed through the center of the interconnector. Copper connectors are attached to the top of the p-type semiconductor and bottom of n-type semiconductor. The dimensions of the model are given in Table [1].

Table 1: Dimensions of the model

Dimension	Value	Units
W	5	mm
D	5	mm
H_N	5	mm
H_L	5	mm
H_I	5	mm
W_{In}	5	mm
D_{In}	3	mm
H_{In}	8	mm
L_V	0.5	mm
W_V	0.1	mm
H_V	2	mm

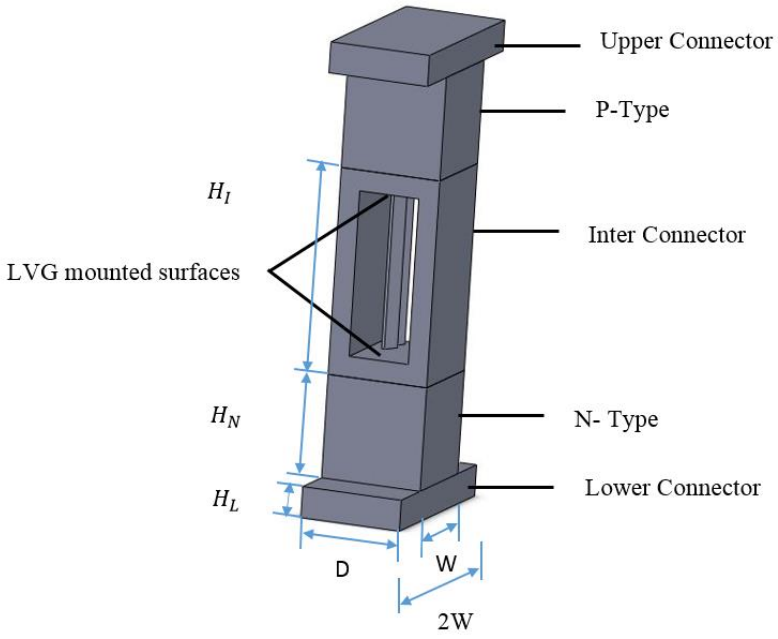

FIGURE 1: Thermoelectric leg model with LVGs. The hot gas passes through the center of the interconnector, and the LVGs are used to increase heat transfer from the gas to the thermoelectric legs

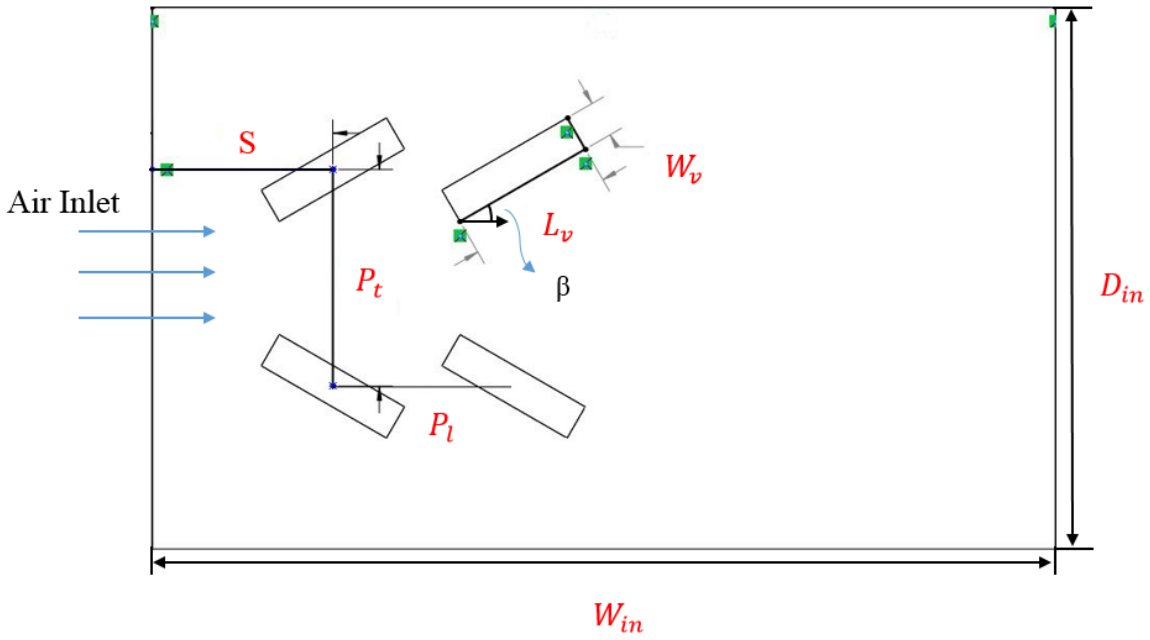

FIGURE 2: Schematic diagram of the placement of LVGs in the flow channel

The p-type and n-type semiconductor elements have a square cross-section with a height of H_N, while the copper interconnectors have a square cross-section extending up to a height of H_I. The flow channel through the interconnector has a size of W_{In} x D_{In} x H_{In}. The copper connectors have a rectangular cross-section with a height of H_L. LVGs are mounted on top and bottom faces of the inner flow channel as shown in Figure 1. The LVGs have rectangular cross section and a height of H_V with an angle of 30° as shown in Figure 2. Ma et al. [16] demonstrated that setting the height of the LVG, H_V, equal to the full height of inner flow channel gave maximum thermal efficiency and power output. Therefore, here the configuration having H_V equal to the full height of the inner channel is modeled. Other important geometrical parameters including the transverse pitch between the adjacent LVGs, P_t, the longitudinal pitch, P_l, and the distance from inner flow channel inlet to the mid-point of the closest pair of LVGs, s, are also shown in Figure 2.

In the simulations, temperature dependent physical properties are considered for both copper and the thermoelectric materials [13, 17]. The n-type semiconductor has 75% Bi_2Te_3 and 25% Bi_2Se_3 and the p-type semiconductor has 25% Bi_2Te_3 and 75% Bi_2Se_3 (1.75 % excess Se).

The numerical simulation domain and boundary conditions are shown in Figure 3. The hot air enters from the left side of the figure and exits from the right side, and the physical properties of air are assumed to be constant. The inlet and the outlet of the flow channel extends 5 times and 20 times the width of the inner flow channel, respectively, in order to maintain uniform flow at the inlet and to suppress backflow at the outlet. The temperature of air entering the inlet flow channel, T_h, is taken to be 550 K. The top surface of the upper copper connector and the bottom surface of the lower copper connector are maintained at 300 K which is denoted by T_c. The left side of the upper copper connector is kept at 0 V and distributive impedance with an optimal load resistance of $4.88\times10^{-8}\ \Omega\, m^2$ is applied on the right side of the lower connector. Adiabatic boundary conditions are assumed on the remaining outer surfaces.

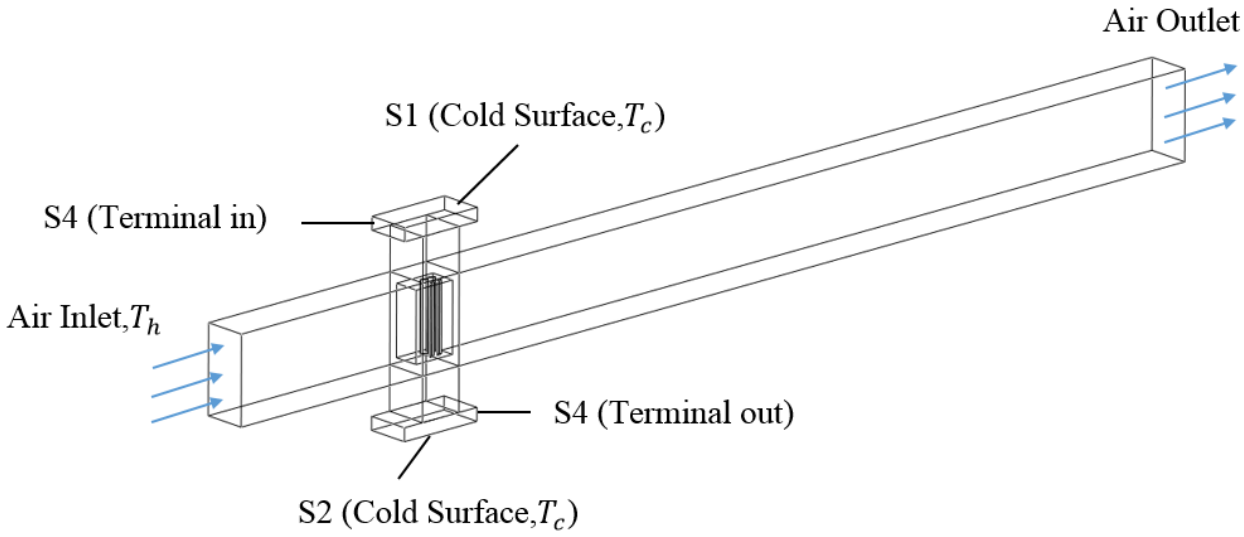

FIGURE 3: Numerical simulation domain and boundary conditions

Numerical Model and Data Reduction

The flow through flow channel is assumed to be three dimensional, laminar, incompressible, and steady. Our assumption of steady flow is supported by a computational study conducted by Sohankar and Davidson [18]. They analyzed three dimensional unsteady laminar flow and heat transfer in a channel with LVGs and showed that the flow is steady for $Re < 1000$. In our case, flows between Re = 100 to 500 are analyzed, so it is safely assumed that the flow is steady. The continuity, momentum and energy equations are as follows:

$$\rho_f \nabla . u = 0 \qquad (2)$$

$$\rho_f (u . \nabla u) = -\nabla p + \mu_f . \nabla^2 u \qquad (3)$$

$$\rho_f \, c_p u \, . \nabla T = \nabla . (k_f \nabla T) \qquad (4)$$

where ρ_f is density, μ_f is dynamic viscosity, p is static pressure, c_p is heat capacity, k_f is thermal conductivity, and u is the velocity of the fluid.

COMSOL Multiphysics®, a commercial software package, is used to incorporate thermoelectric effects in the model. This software solves the governing equations based on a finite element method.

In COMSOL Multiphysics®, the thermoelectric module mainly consists of three important thermoelectric effects: the Seebeck, Peltier, and Thompson effects. The Seebeck effect describes the generation of a voltage from a temperature gradient across the material. The Peltier effect results in the production or absorption of heat at a junction between two different thermoelectric materials when an electric current flows through the junction. The Thomson effect describes the production or absorption of heat along a conductor with a temperature gradient when an electric current flows through the material. Considering the case of temperature dependent material properties and neglecting any heat loss outside the solid thermoelectric legs (the outer walls of the thermoelectric elements, the copper interconnector section, and the top and bottom copper connector sections), the energy balance equation of the thermal field is given by,

$$\nabla q_{p,n} = -\nabla\left[\mathrm{k}_{p,n}(T_{p,n})\,\nabla \mathrm{T}_{p,n}\right] \tag{5}$$

$$\nabla q_{p,n} = m_{p,n}c_{p,n}\frac{\partial T_{p,n}}{\partial t} + J^2\rho_{p,n}(T_{p,n}) + \left[\nabla \alpha_{p,n}(T_{p,n})\right]T_{p,n}\,J \tag{6}$$

where the first term on right side is the transient term (which is neglected in this paper, as only steady state conditions are examined), the second term is the joule heating term, and third source term is from the Peltier and Thomson effects. In the above equations, the subscripts p and n represent p-type and n-type semiconductors, respectively. In these equations, $\nabla q_{p,n}$ denotes heat conduction. The governing equation for the electric field is written as follows:

$$\nabla \mathrm{V} = -\alpha_{p,n}(T_{p,n})\,\nabla T_{p,n} - \rho_{p,n}(T_{p,n})J \tag{7}$$

where the first term on right side indicates Seebeck electromotive force and the second term indicates voltage drop due to current flow. The flux charge conservation equation is given by:

$$\nabla \cdot \mathrm{J} = 0 \tag{8}$$

The multiphysics software, COMSOL Multiphysics® 4.4, is set to use a geometric multigrid iterative solver for fluid flow calculations, and an algebraic multigrid solver for heat transfer and electric current calculations. The criteria of convergence for residual for every variable should be less than 10^{-5}. The Reynolds number is calculated from

$$\mathrm{Re} = \frac{\rho_f U D_h}{\mu} \tag{9}$$

where D_h is the hydraulic diameter based on the inlet rectangular channel, U is the inlet velocity, and ρ_f and μ_f are the density and dynamic viscosity, respectively.

Net power,W_{net} supplied by the thermoelectric generator can be calculated as a difference of total power output,P_o and pumping power$W_{\Delta p}$.

$$W_{\text{net}} = P_0 - W_{\Delta p} \quad (10)$$

$$W_{\Delta p} = \dot{V}.\,\Delta p \quad (11)$$

where $\dot{V}$ is volumetric flow rate and p is the static pressure.

The thermal conversion efficiency of thermoelectric generator is given by

$$\eta = \frac{W_{net}}{Q_h} \quad (12)$$

where Q_h is the heat input to the TEG.

Grid Independence and Code Validation

The mesh grid is generated in COMSOL Multiphysics® and scaled to align with the geometrical units. Both the thermal and electrical analysis use the same grid, thus they have same 3D coordinate system with regard to the cells and boundary walls of the domain. The angle of attack between the length direction of the rectangular LVG and the main flow direction makes the geometrical structure of the fluid flow field more complex. Unstructured meshes generated near the wall of the LVGs and the copper connector are fine enough and inflation layers close to the wall are sufficient to capture the wall effects and thermal boundary layer phenomena.

The results are verified for independence with respect to the mesh, in order to ensure accuracy of the simulations. Four grid levels were studied with number of elements ranging from 2×10^5 to 5×10^6 for thermoelectric generators with LVGs of H = 4 mm and β= 45° at Re = 500. Figures [4-6] demonstrate that the results are independent of the grid size once the grid reaches 2 million mesh elements. Thus, considering the calculation duration and the availability of resources, 2.5 million cells are selected as the final grid for later calculations.

The numerical method has been validated with the thermoelectric generator and fluid flow channel by comparing results with those from Reddy et al. [17] for a model without LVGs in the flow field. Figures [7] and [8] demonstrate that our results agrees well those from Reddy et al. [17].

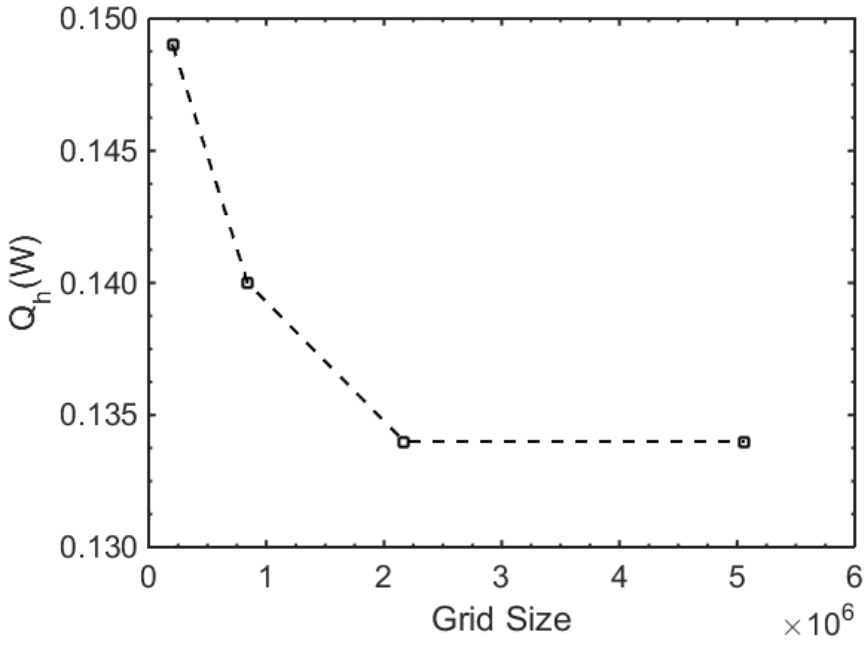

FIGURE 4: Grid independence for heat input

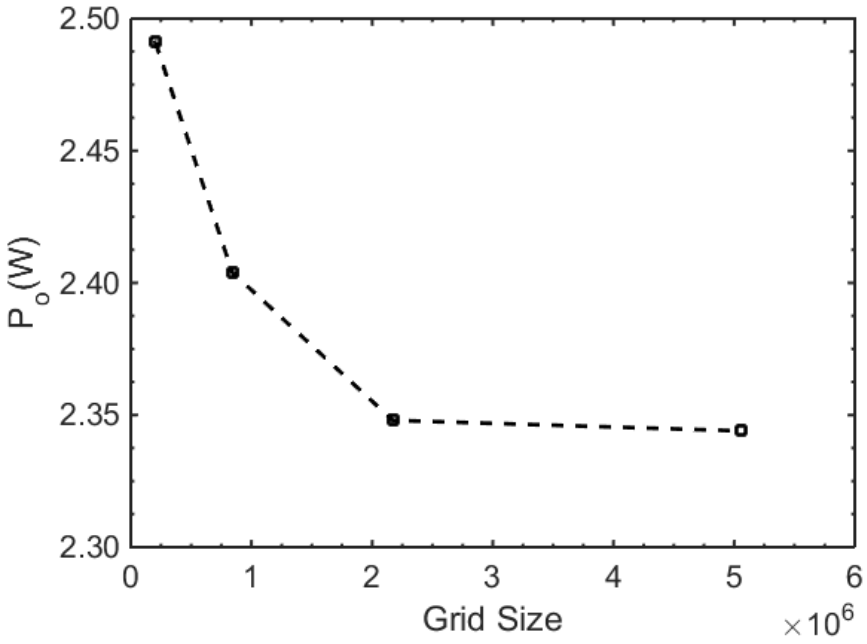

FIGURE 5: Grid independence for power output

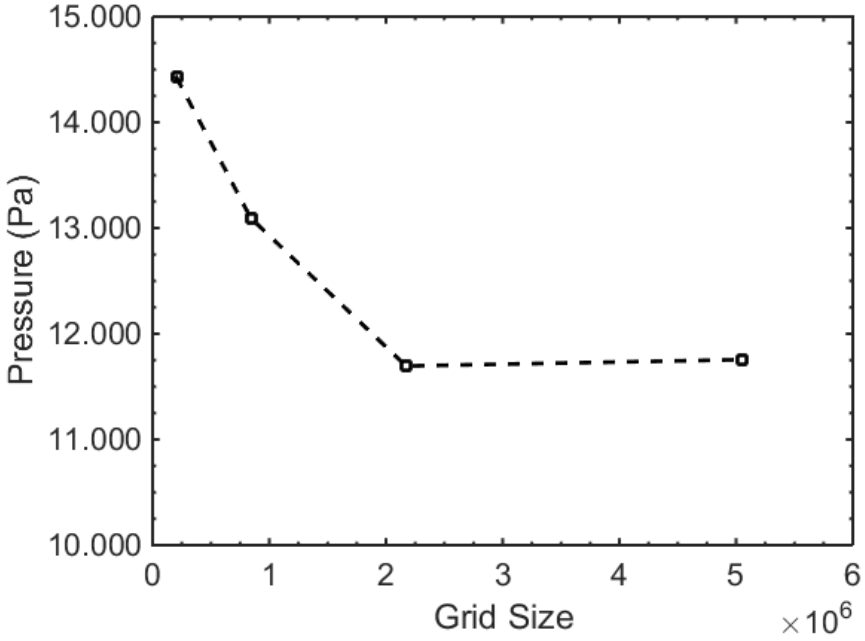

FIGURE 6: Grid independence for pressure

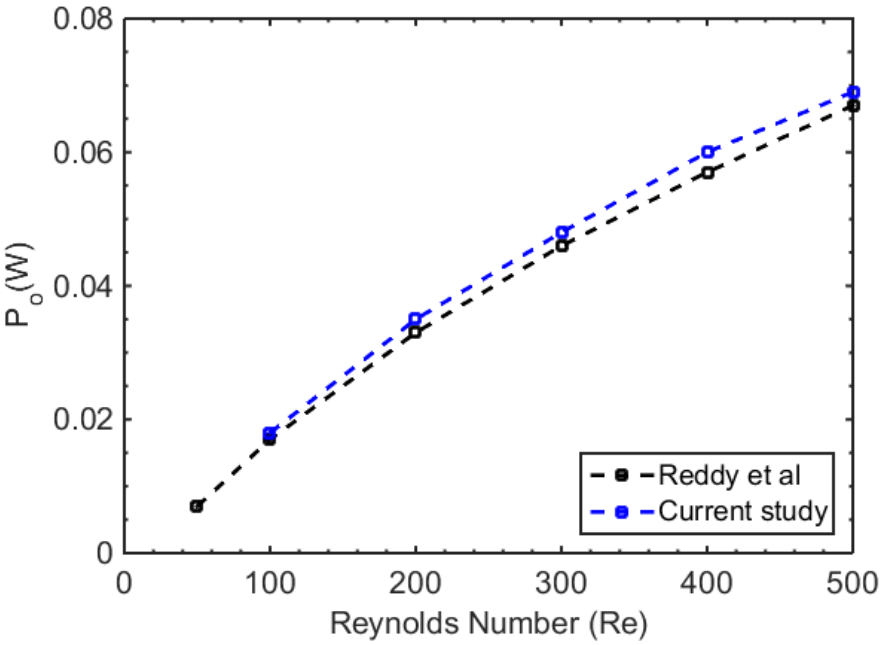

FIGURE 7: Power output as a function of Reynolds number for a benchmark case. The results are nearly identical to those from Reddy et al. [17]

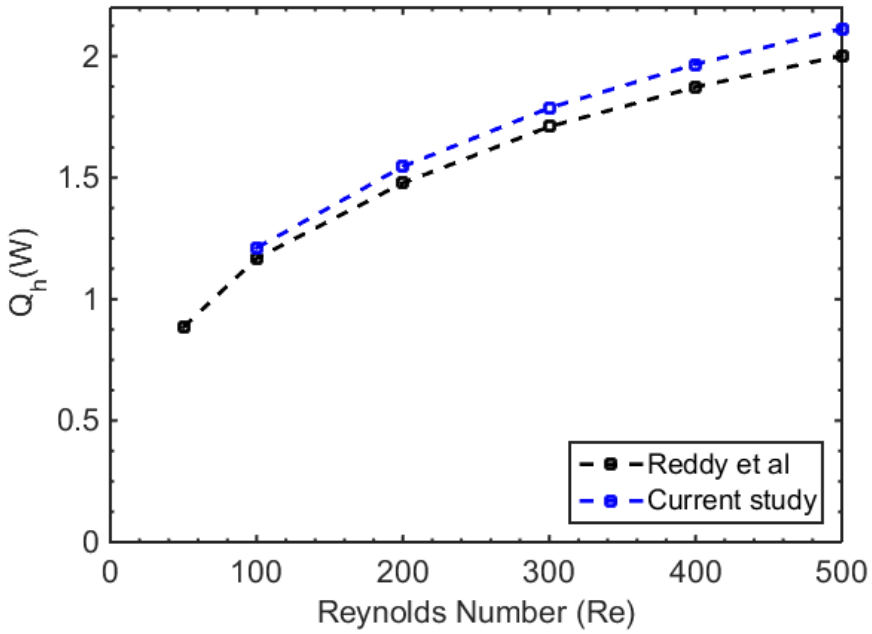

FIGURE 8: Heat input as a function of Reynolds number in comparison with results from Reddy et al [18].

RESULTS AND DISCUSSION

Effect of Longitudinal Vortex Generator Location

Longitudinal vortices primarily influence heat transfer downstream of the LVG. A comparison between a model with LVGs and same model without LVGs shows that heat transfer increases by an average percent difference of 32.50 % as shown in Figure 9.

Thus, it follows that the location of the LVG in the channel will influence the global heat transfer for that channel. In this section, the effects of varying the LVG location on the heat input and the pressure drop of the thermoelectric generator are examined. The location of the LVG is described by the parameters s and P_l, where s represents the location of the mid-point of the first pair of LVGs from the front edge, and P_l, is the longtudinal pitch. In the following computations the Reynolds number varies from 100 to 500.

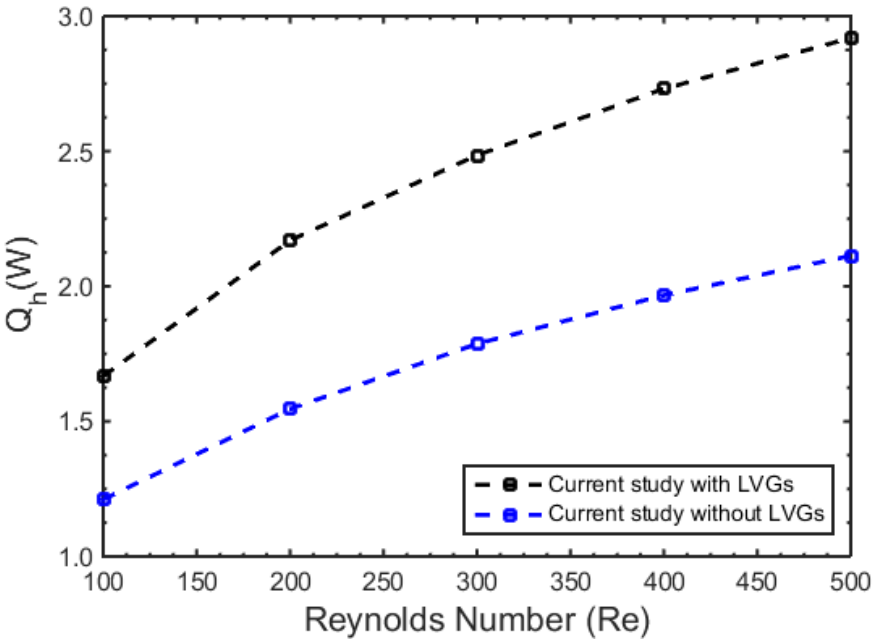

FIGURE 9: Comparison between heat input with a model with LVGs and same model without LVGs. The results enhancement in heat transfer due to LVGs.

With P_l = 1 mm, the average heat input for varying LVG distance from the inlet is shown in Figure 10. As the LVG moves away from the inlet of the channel (increasing value of s), the heat transfer enhancement remains relatively constant. For LVGs located close to leading edge, one might expect the heat input to be the greatest as the vortices generated travel a greater distance across the surface of the channel. However, our results show that the heat input is relatively independent of this distance. One possible reason to explain this behavior could be that while the vortices do increase the heat transfer overall (as seen in the difference between Figure 9), the effect of vortices generated in this study are restricted by short streamwise distance after the LVGs. Future work will examine methods to increase the effects of the LVGs through changes in the inner flow channel geometry or geometry of LVGs. For a fixed LVG location, the heat input increases with increasing Reynolds number. However for large Reynolds number the heat input increases slowly.

An anomaly is observed in the heat input at the location s = 2 mm. At this location, there is a slight, but sudden increase in heat input. In order to confirm the existence of this anomaly, the model was simulated in two different software packages, COMSOL Multiphysics® and ANSYS FLUENT.

Also, the results were checked for various grid sizes ranging from 2×10^5 to 5×10^6. This anomaly existed regardless of the solver and mesh.

In an attempt to understand the sudden rise of the heat input at this location, the corresponding velocity profiles of the middle cross sections of the thermoelectric modules were calculated and are shown in Figure 11. These velocity plots give an indication of the degree of fluid mixing, where the mixing could disrupt the thermal boundary layer and thus enhancing the heat transfer. However, from these velocity profiles, the origin of the anomaly is not entirely clear. It does appear as though the fluid velocity around the LVGs is slightly greater for s = 2.0, but it is not clear why the flow would speed up at only this location.

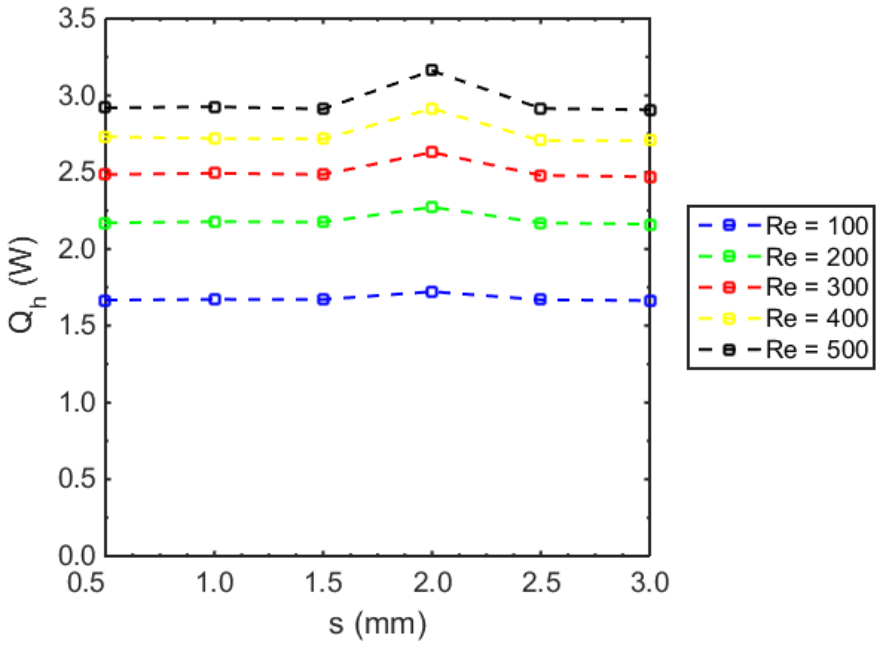

FIGURE 10: Heat input as a function of the distance, s, that the LVG is placed from the leading edge of the channel.

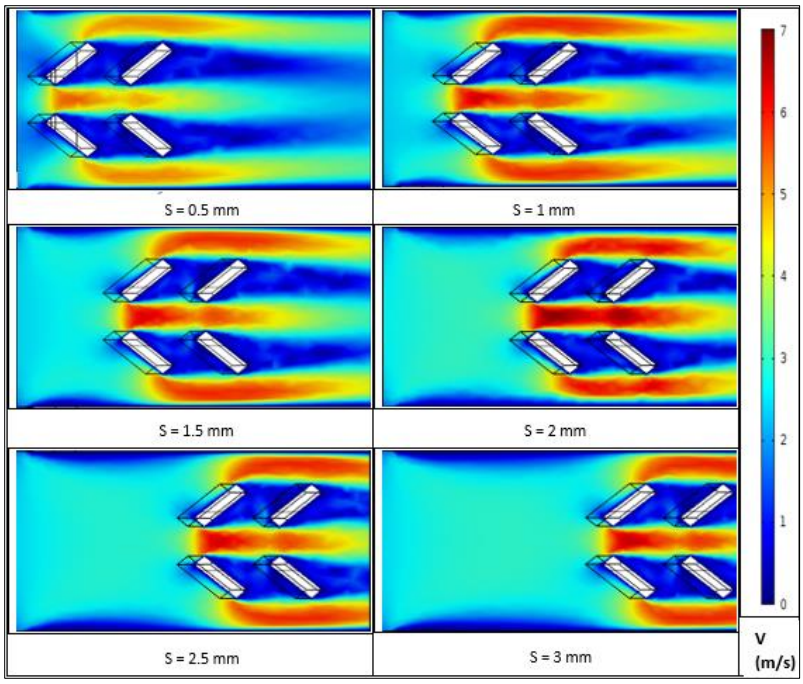

FIGURE 11: Velocity profile of the middle cross sections of the thermoelectric modules for various LVG locations at Re = 500

With regard to the pressure drop in the channel, the numerical results show that the distance, *s*, between the leading edge of the channel and the LVG has little effect on the total flow loss of the channel (with the exception of s = 2 mm at high Reynolds numbers) as shown in Figure 12. However as shown in Figure 13, the rectangular winglet pair does create extra pressure drop due to its form drag. There is a steep pressure drop that occurs at the inlet of the channel, and a much greater pressure drop occurs at the LVG. Once the flow passes the LVG, the fluid pressure rises again because of the increase in the cross section flow area, and the pressure then decreases gradually as the flow passes through the remainder of the channel.

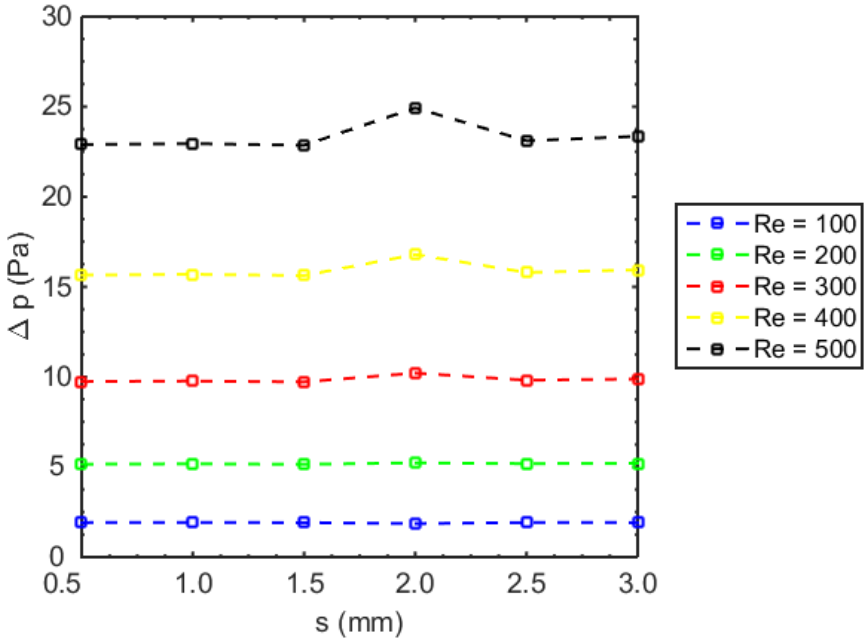

FIGURE 12: Pressure drop as a function of the LVG distance from the leading edge of the channel.

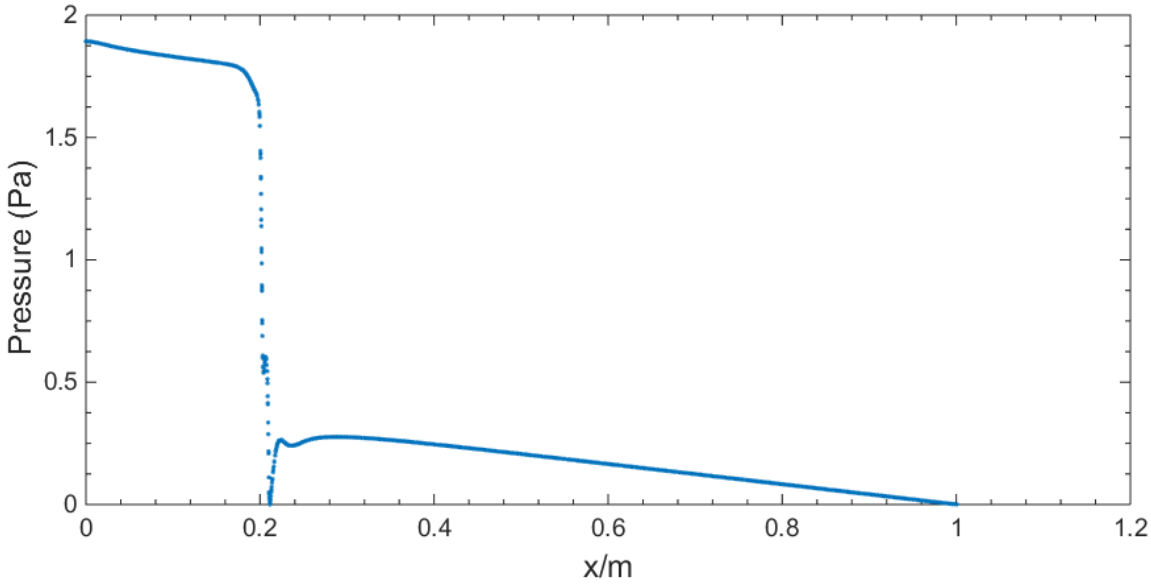

FIGURE 13: Pressure drop across the whole fluid domain along the central line.

The effect of the LVG location on the net power output of the thermoelectric generator is presented in Figure 14. As with the heat input, the LVGs also slightly improve the net power output when close to the inlet of the channel for a fixed Reynolds number. Similarly, as the Reynolds number

increases, the heat input and the net power output of the system also increase. Since the Seebeck voltage is proportional to the temperature difference between the hot and the cold sides of the thermoelectric modules, it follows that the output power should increase given the increases in the heat input. However, as noted earlier, the increase in the heat input with the LVGs comes with the penalty of additional pressure drop. This additional pressure drop requires an increase in the pumping power. Thus, the ratio of the pumping power to the power output is plotted in Figure 15 and the ratio is always very small, thus showing that the pumping power is much less than the power output for all the cases. Therefore the net power is almost the same as the power output.

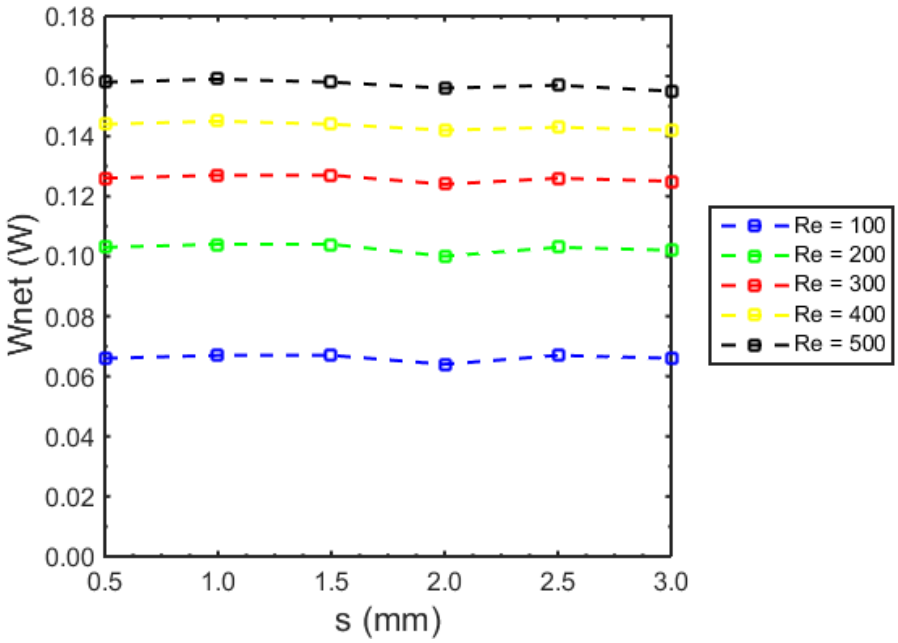

Figure 14: Net power output of the thermoelectric generator as a function of the LVG distance from the leading edge of the channel.

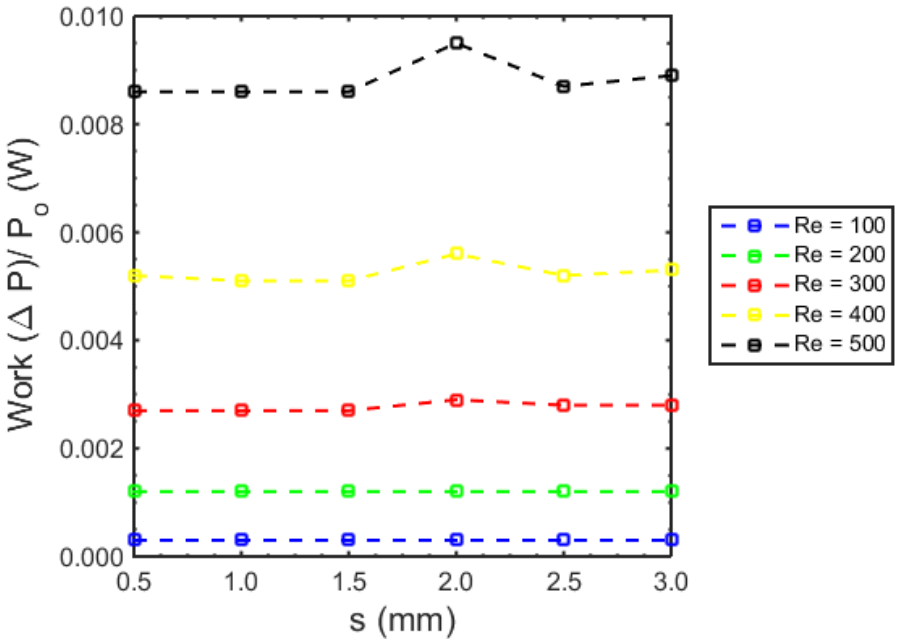

FIGURE 15: Ratio of pumping power to power output as a function of the LVG distance from the leading edge of the channel. The increase in pumping power is only a small fraction of the total thermoelectric power produced.

The thermal efficiency of the thermoelectric system is shown in Figure 16. As expected, the thermal efficiency remains roughly constant with the exception of the anomaly at s=2 mm as discussed previously.

Effect of Longitudinal Pitch

In addition to examining the distance between the LVGs and the leading edge of the channel, also examined was the effect of the longitudinal pitch, P_l, between the pairs LVGs in the streamwise direction (see Figure. 2). Figure 17 shows the heat input for two different pitches as a function of distance from the leading edge of the channel. The streamwise location of the first pair of LVGs varies from s = 0 – 1.5 mm in steps of 0.5 mm, while the size of the LVGs is kept constant and the Reynolds number is fixed at Re = 400. The heat transfer has been marked for two different values, P_l = 1 mm and P_l = 2 mm. The results show a small, but consistent, increase of about 4 % in the heat input for the larger pitch. However, while the increased longitudinal pitch increases the heat input, there is also a corresponding increase in the pressure drop as shown in shown in Figure 18.

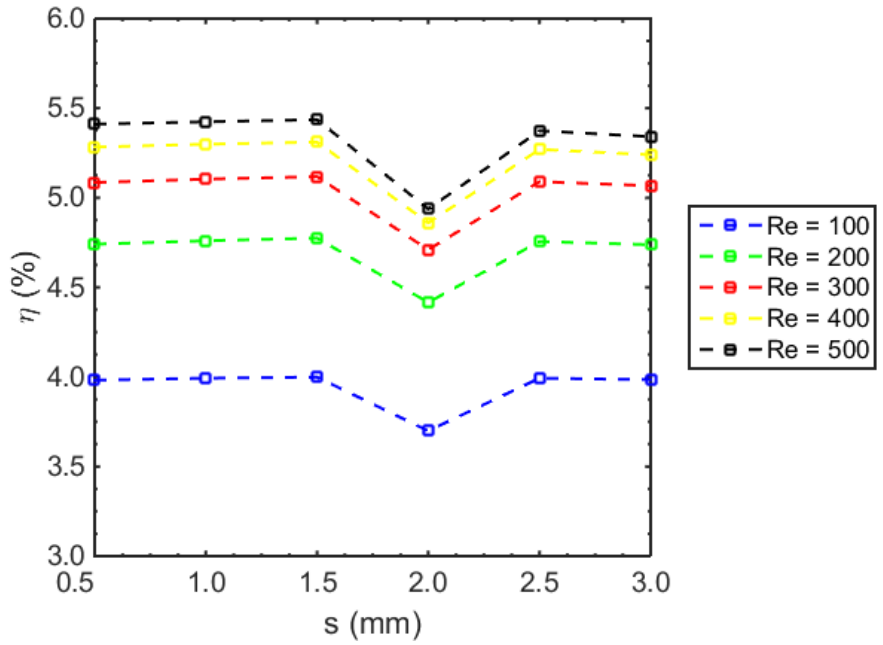

FIGURE 16: Thermal efficiency of the thermoelectric generator as a function of the LVG distance from the leading edge of the channel.

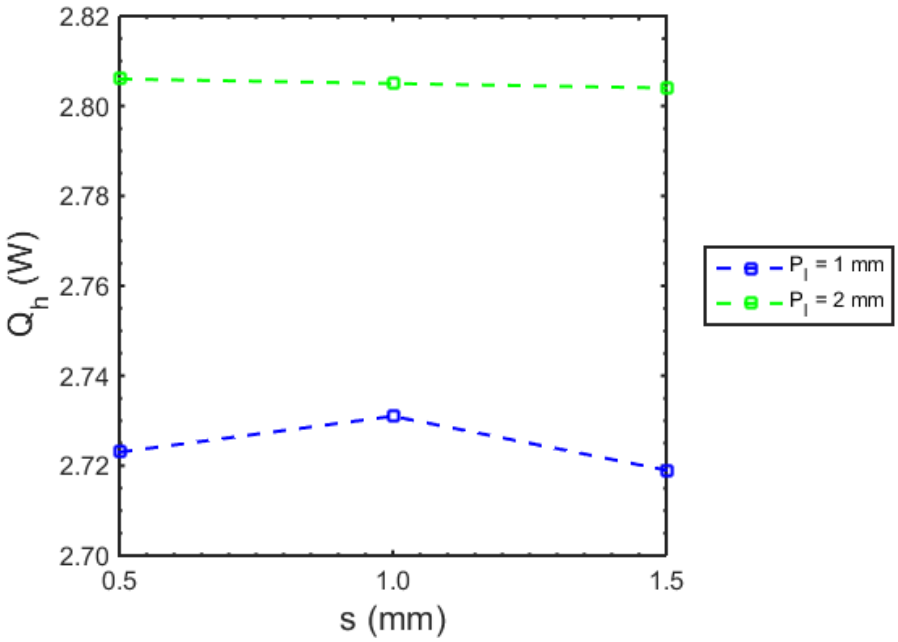

FIGURE 17: Heat input as a function of distance from the leading edge of the channel for pitch distances of 1 and 2 mm and a Reynolds number of 400.

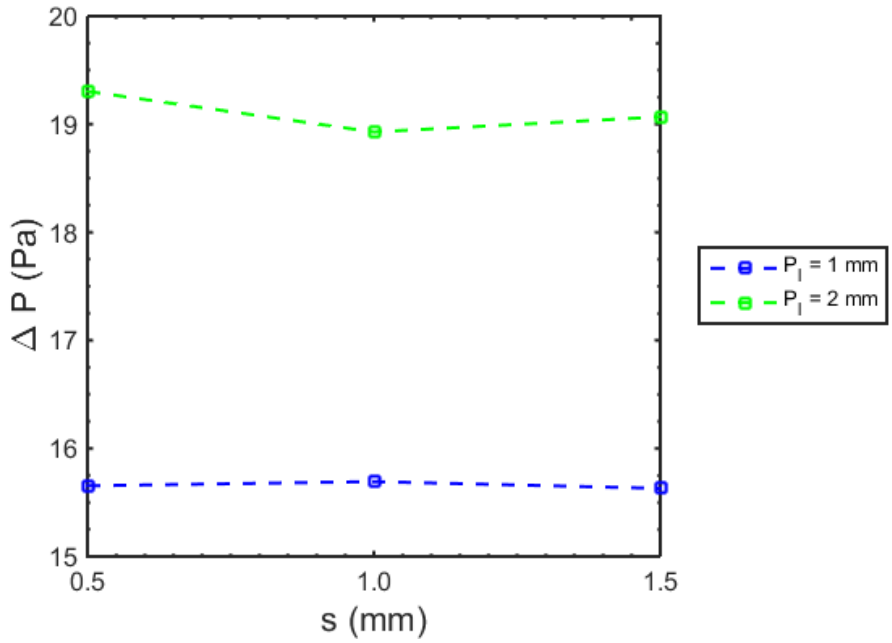

FIGURE 18: Pressure drop as a function of distance from the leading edge of the channel for pitch distances of 1 and 2 mm and a Reynolds number of 400.

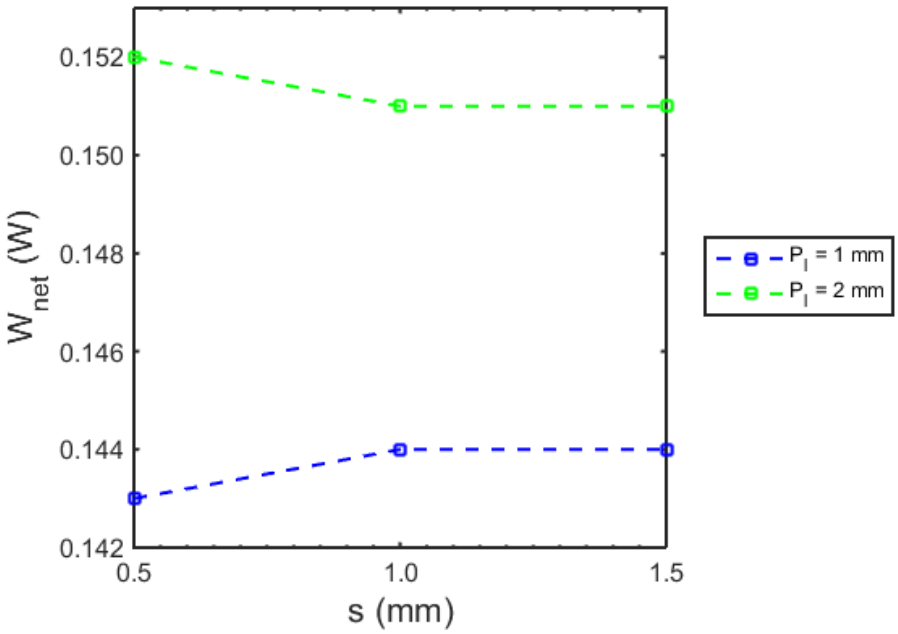

FIGURE 19: Power output as a function of distance from the leading edge of the channel for pitch distances of 1 and 2 mm and a Reynolds number of 400.

The effect of the longitudinal pitch on the net power output of the thermoelectric generator is presented in Figure 19. As the heat input is enhanced with the increase in longitudinal pitch, the net power output also increases slightly. Given the small increases in heat input and power output, the thermal efficiency exhibits a slight, but consistent, improvement as seen in Figure 20.

CONCLUSION

In this paper, the effect of the location and longitudinal pitch of LVGs was analyzed on the heat transfer, pressure drop, and power output for a thermoelectric generator. A fluid – thermal – electric multiphysics coupled model was established using COMSOL Multiphysics software. In this study, the thermoelectric model included Joule, Seebeck, Peltier and Thomson effects along with temperature dependent material properties. The main conclusions of this work are summarized as follows:

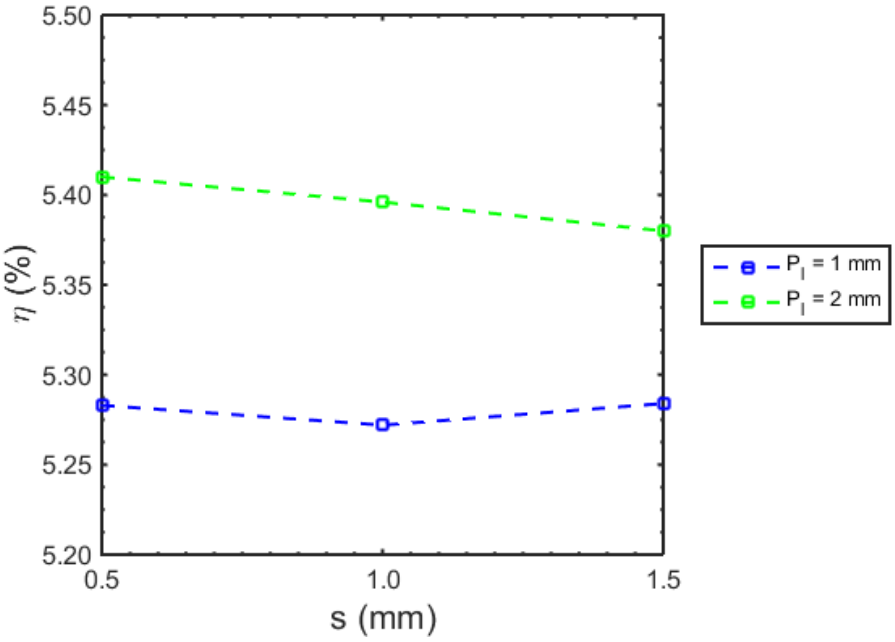

FIGURE 20: Thermal efficiency as a function of distance from the leading edge of the channel for pitch distances of 1 and 2 mm and a Reynolds number of 400.

- LVGs enhance the heat transfer to the thermoelectric device, however they also increase the pressure drop slightly. As the distance of the LVG from the leading increases, the heat input,

power output, and thermal efficiency were found to remain relatively constant, with one exception noted below.

- An anomaly in the heat input and pressure drop was observed when the first pair of LVGs was located at a distance of s = 2 mm from the leading edge. The origin of this anomaly is unclear although it may be speculated that it might be due to a Venturi effect. However, it is not clear what would cause the Venturi effect at only this location.
- The effect of longitudinal pitch is small, but potentially significant. With the chosen geometry, the increases in heat transfer with increasing pitch were modest. However, this work shows that it is important to have the pairs of LVGs separated enough such that the individual effects of each pair are maximized.

ACKNOWLEDGEMENTS

This material is based upon work supported by the National Science Foundation and Department of Energy through the NSF/ DOE Joint Thermoelectric Partnership, Grant No. CBET-1048708.

REFERENCES

[1] Karim, A. M., Federici, J. A., and Vlachos, D. G., 2008, "Portable power production from methanol in an integrated thermoeletric/microreactor system," Journal of Power Sources, 179(1), pp. 113-120.

[2] Yang, J., 2005, "Potential Applications of Thermoelectric Waste Heat Recovery in the Automotive Industry," Thermoelectrics, 2005. ICT 2005. 24th International Conference on. IEEE, 2005.

[3] Espinosa, N., Lazard, M., Aixala, L., and Scherrer, H., 2010, "Modeling A Thermoelectric Generator Applied To Diesel Automotive Heat Recovery," Journal of Electronic Materials, 39(9), pp. 1446-1455.

[4] Saqr, K. M., Mansour,M. K. , Musa,M. N., 2008, "Thermal Design Of Automobile Exhaust Based Thermoelectric Generators: Objectives And Challenges" International Journal of Automotive Technology, 9(2) pp. 155-160.

[5] Zorbas, K. T., Hatzikraniotis, E., and Paraskevopoulos, K. M., 2007, "Power and Efficiency Calculation in Commercial TEG and Application in Wasted Heat Recovery in Automobile," Proc. of 5th European Conference on Thermoelectrics.

[6] Pandit, J., Thompson, M., Ekkad, S. V., Huxtable,S., 2013, "Experimental Investigation Of Heat Transfer Across A Thermoelectric Generator For Waste Heat Recovery From Automobile Exhaust," Proceedings of the ASME 2013 Heat Transfer Summer Conference.

[7] Hsiao, Y. Y., Chang, W. C., and Chen, S. L., 2010, "A Mathematic Model of Thermoelectric Module with Applications on Waste Heat Recovery from Automobile Engine," Energy, 35(3), pp. 1447-1454.

[8] Wang, X., Huang, Y., Cheng, C., Lin, D. T., and Kang, C., 2012, "A Three-Dimensional Numerical Modeling of Thermoelectric Device with Consideration of Coupling of Temperature Field and Electric Potential Field," Energy, 47(1), pp. 488-497.

[9] Chen, M., Rosendahl, L. A., and Condra, T., 2011, "A three-dimensional numerical model of thermoelectric generators in fluid power systems," International Journal of Heat and Mass Transfer 54 pp. 345–355.

[10] Reddy, B. V. K., Barry, M., Li, J., and Chyu, M. K., 2014, "Convective Heat Transfer and Contact Resistances Effects on Performance of Conventional and Composite Thermoelectric Devices," Journal of Heat Transfer, 136(10), p. 101401. Reddy, B. V. K., Barry, M., Li, J., and Chyu, M. K., 2013, "Thermoelectric Performance of Novel Composite and Integrated Devices Applied to Waste Heat Recovery," Journal of Heat Transfer, 135(3), p. 031706.

[11] Reddy, B. V. K., Barry, M., Li, J., and Chyu, M. K., 2014, "Thermoelectric-Hydraulic Performance of a Multistage Integrated Thermoelectric Power Generator," Energy Conversion and Management, 77, pp. 458-468.

[1] Pandit, J., Thompson, M., Ekkad, S. V., and Huxtable, S., 2014, "Effect of Pin Fin to Channel Height Ratio and Pin Fin Geometry on Heat Transfer Performance for Flow in Rectangular Channels," International Journal of Heat and Mass Transfer, 77, pp. 359-368.

[2] Tiggelback, S., Mitra,N.K. ,Fiebig,M. , 1993, "Experimental Investigations Of Heat Transfer Enhancemnet And Flow Losses In A Channel With Double Rows Of Longitudinal Vortex Generators " International Journal of Heat and Mass Transfer, 36(9), pp. 2327-2337.

[3] Wu, J. M., and Tao, W. Q., 2008, "Numerical Study on Laminar Convection Heat Transfer in a Channel with Longitudinal Vortex Generator. Part B: Parametric Study of Major Influence Factors," International Journal of Heat and Mass Transfer, 51(13-14), pp. 3683-3692.

[4] Ma, T., Pandit, J., Ekkad, S. V., Huxtable, S. T., and Wang, Q., 2015, "Simulation of thermoelectric-hydraulic performance of a thermoelectric power generator with longitudinal vortex generators," Energy, 84, pp. 695-703.

[5] Reddy, B. V. K., Barry, M., Li, J., and Chyu, M. K., 2012, "Three-Dimensional Multiphysics Coupled Field Analysis of an Integrated Thermoelectric Device," Numerical Heat Transfer, Part A: Applications, 62(12), pp. 933-947.

[1] Davidson, A. S. L., 2001, "Effect of inclined vortex generators on heat transfer enhancement in a three-dimensional channel." Numerical Heat Transfer: Part A: Applications, 39(5), pp. 433-448.